Scenario Choice Impacts Carbon Allocation Projection at Global Warming Levels

Lee de Mora[1], Ranjini Swaminathan[2], Richard P. Allan[2], Jeremy Blackford[1], Douglas I. Kelley[3], Phil Harris[3], Chris D. Jones[4], Colin G. Jones[5], Spencer Liddicoat[4], Robert J. Parker[6,7], Tristan Quaife[2], Jeremy Walton[4], and Andrew Yool[8]

[1]Plymouth Marine Laboratory, Plymouth, PL1 3DH
[2]National Centre for Earth Observation and Department of Meteorology, University of Reading, Reading, UK
[3]UK Centre for Ecology & Hydrology, Wallingford, Oxfordshire, OX10 8BB, UK
[4]Met Office Hadley Centre for Climate Science and Services, Exeter, EX1 3PB, UK
[5]National Centre for Atmospheric Science, UK, and School of Earth and Environment, University of Leeds, Leeds, UK
[6]National Centre for Earth Observation, Space Park Leicester, University of Leicester, Leicester, UK
[7]Earth Observation Science, School of Physics and Astronomy, University of Leicester, UK
[8]National Oceanography Centre, European Way, Southampton, SO14 3ZH, UK

Correspondence: Lee de Mora (ledm@pml.ac.uk)

Abstract.

We show that the distribution of anthropogenic carbon between the atmosphere, land surface and ocean differs with the choice of projection scenario even for identical changes in mean global surface temperature. Warming thresholds occur later in lower carbon dioxide (CO_2) emissions scenarios and with less carbon in the three main reservoirs than in higher CO_2 emissions scenarios. At 2 °C of warming, the mean carbon allocation differs by up to 63 PgC between scenarios and this is equivalent to approximately six years of current global total emissions. At the same warming level, higher CO_2 concentration scenarios have a lower combined ocean and land carbon allocation fraction of the total carbon compared to lower CO_2 concentration scenarios.

The warming response to CO_2, quantified as the equilibrium climate sensitivity, ECS, directly impacts a models global warming threshold exceedance year and hence the carbon allocation. Low ECS models have more carbon than high ECS models at a given warming level because the warming threshold occurs later, allowing more emissions to accumulate.

These results are important for carbon budgets and mitigation strategies as they impact how much carbon the ocean and land surface could absorb at a given warming level. Carbon budgeting will be key for reducing the impacts of anthropogenic climate change, and these findings could have critical consequences for policies aimed at reaching net zero.

Keywords: Climate change, Carbon Cycle, Carbon Allocation, CMIP6, Earth System Models

1 Introduction

The Intergovernmental Panel on Climate Change (IPCC) Sixth Assessment Report found that the global mean surface air temperature was 1.1°C warmer in the recent decade (2011-2020) than in the pre-industrial era. They found that human activities

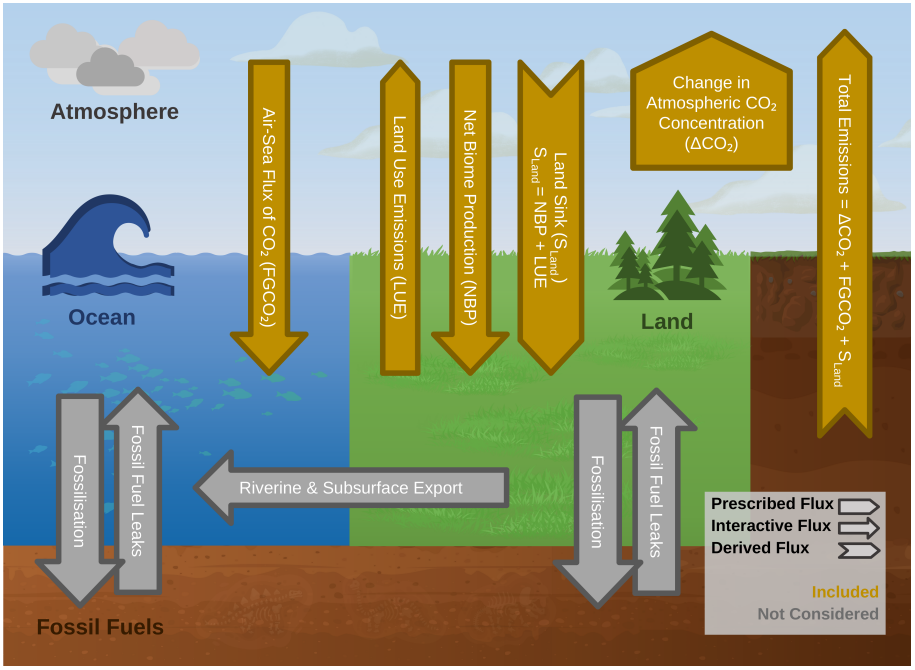

Figure 1. A simplified version of the Earth System carbon cycle. Interactive fluxes are shown as arrows, prescribed fluxes are shown as box arrows, and derived fluxes are shown as chevrons. The arrows in gold are considered in this analysis, and the grey arrows are not considered. The prescribed change in atmospheric carbon, ΔCO_2, accounts for the anthropogenic fossil fuel exploitation and the subsequent carbon emission.

have indisputably caused this warming (IPCC, 2021b), with anthropogenic greenhouse gases, particularly carbon dioxide (CO_2), being the primary cause.

Since the advent of the industrial revolution, carbon has been transferred gradually from fossil fuel reservoirs to the atmosphere, primarily via combustion. Once in the atmosphere, some of the CO_2 is absorbed by the ocean via gas transfer, some is absorbed by the land surface via terrestrial carbon fixation, while some CO_2 remains in the atmosphere, as illustrated in Fig. 1. While these fluxes also occur naturally, the additional anthropogenic carbon load has perturbed the Earth System from its pre-industrial equilibrium. In the atmosphere, anthropogenic carbon causes additional warming (Hansen et al., 1981). In the ocean, anthropogenic carbon can cause acidification (Caldeira and Wickett, 2003) or participate in primary production or sequestration (Schlunegger et al., 2019). On the land surface, carbon can allow enhanced primary production and subsequent carbon sequestration. Once converted into biomass, this carbon may be a fuel source in fires which returns a portion of the sequestered carbon back to the atmosphere (Burton et al., 2022; Sullivan et al., 2022). Elevated atmospheric CO_2 can worsen food quality and nutrient concentrations (Erda et al., 2005), and affect water-balance evapotranspiration, reducing streamflow in water-stressed regions (Ukkola et al., 2016).

The instantaneous distribution of anthropogenic carbon between the atmosphere, ocean and land surface is known as "carbon allocation in the Earth System" which we henceforth call "carbon allocation". The balance between these carbon sinks is hugely important to climate projections and policymakers (IPCC, 2021b), impacting warming feedbacks, marine biogeochemistry and life on land (Macreadie et al., 2019; Hilmi et al., 2021). The physical and biogeochemical feedbacks could affect the future rates of greenhouse gas accumulation in the atmosphere, directly impacting warming (Canadell et al., 2021). They also directly influence the remaining carbon budget, which policymakers may use to limit fossil fuel consumption in order to keep warming in line with policy goals (Jiang et al., 2021). In addition, the balance of carbon between the atmosphere, land and ocean has large-scale consequences on the future of climate engineering via CO_2 removal and solar radiation modification (Lawrence et al., 2018). Changes to carbon allocation also impact several United Nations Development Programme Sustainable Development Goals, notably 13: Climate Action, 14: Life below Water and 15: Life on Land (United Nations, 2015).

In observations, the atmospheric CO_2 concentration is typically measured directly, while the ocean and terrestrial CO_2 sinks are estimated with global process models constrained by observations. For the decade 2008–2017, the Le Quéré et al. (2018) synopsis of the global carbon budget summarised that the fossil fuel emissions were 9.4 ± 0.5 PgC yr^{-1}, and emissions from land use and land-use change was 1.5 ± 0.7 PgC yr^{-1}, most of which was due to deforestation. The growth of the atmospheric carbon was 4.7 ± 0.02 PgC yr^{-1}, the ocean carbon sink was 2.4 ± 0.5 PgC yr^{-1}, and the terrestrial carbon sink was 3.2 ± 0.8 PgC yr^{-1}. The difference between the estimated total emissions and the estimated changes in the atmosphere, ocean, and terrestrial biosphere was 0.5 PgC yr^{-1}, which indicated that there were either overestimated emissions or underestimated sinks or both. There is also a flux of land carbon into the ocean via rivers between 0.45 ± 0.18 PgC yr^{-1} and 0.78 ± 0.41 PgC yr^{-1}, but this flux is not generally included in CMIP6 models (Jacobson et al., 2007; Resplandy et al., 2018; Hauck et al., 2020). There may also be a direct flux of fossil fuel extraction and other leaks into the ocean or land surface (Roser and Ritchie, 2023), but these are also neglected in models.

It is long established that the relationship between cumulative emissions and peak warming is insensitive to the emission pathway, either in the timing of emissions or the peak emission rate (Allen et al., 2009). More recently, figure 5.31 of Canadell et al. (2021) also shows negligible pathway dependence between the cumulative carbon emissions and the global mean temperature change in several projections.

The rising atmospheric CO_2 and warming climate will cause major changes in vegetation structure and function over large fractions of the global land surface. An increase in global land vegetation carbon has been projected, but with substantial variation between vegetation models (Friend et al., 2014). Much of the variability between models in global land vegetation carbon stocks was explained by differences in land vegetation carbon residence time (Jiang et al., 2015). In the ocean, the increase in atmospheric CO_2 enhances the ocean carbon storage while warming acts to decrease the ocean carbon storage (Katavouta and Williams, 2021).

Both the ocean and land carbon sinks are projected to continue to grow as the atmospheric concentration of CO_2 rises (Canadell et al., 2021). However, the combined fraction of emissions taken up by the land and ocean is projected to decline, and a larger fraction of the emissions will remain in the atmosphere. The carbon allocation at the year 2100 is strongly scenario dependent (IPCC, 2021a, Fig. SPM7). The projected atmospheric carbon allocation in the year 2100 ranges from 30% in SSP1-

1.9 to 62% in SSP5-8.5. The Shared Socioeconomic Pathways (SSPs) are described below in sec. 1.1. While the land and ocean carbon uptake are expected to remain approximately equal, the uncertainty is much larger for the land carbon sink than the ocean. The uncertainty in the land sink is due to the balance of carbon accumulation in the high latitudes against the loss of land carbon in the tropics, and the challenges of forecasting the water cycle, especially droughts, which significantly reduce the carbon absorption potential of the land surface (Ukkola et al., 2016; van der Molen et al., 2011; Canadell et al., 2021). On the other hand, continuous absorption of carbon into the ocean reduces the mean global buffering capacity and drives changes in the global ocean's carbonate chemistry, building a strong dependency on the choice of scenarios (Jiang et al., 2019; Katavouta and Williams, 2021).

1.1 Sixth Coupled Model Inter-comparison Project (CMIP6)

Earth System models (ESMs) are the only tools capable of projecting a future coupled carbon-climate system. The Sixth Coupled Model Inter-comparison Project (CMIP6) is the most recent global effort to standardise, share and study ESM simulations (Eyring et al., 2016). The CMIP6 standard simulation protocols, called the Diagnostic, Evaluation and Characterization of Klima (The DECK), are required simulations for a model to participate in CMIP6. The DECK includes a pre-industrial control, at least one historical simulation, a gradual 1% CO_2 growth experiment and a rapid 4xCO_2 experiment. For quality assurance, only models with a global drift per century lower than 10 PgC in the air-sea CO_2 flux and lower than 0.1 °C in the volume mean ocean temperature are accepted (Jones et al., 2011; Eyring et al., 2016; Yool et al., 2020).

In order to make projections of the future anthropogenic climate drivers, multiple scenarios were proposed in the ScenarioMIP project to cover a wide range of potential futures (O'Neill et al., 2016). ScenarioMIP expands upon the CMIP6 core simulations with multiple scenarios of the future anthropogenic climate drivers that cover a wide range of potential future climate and human behaviours (O'Neill et al., 2016). Scenario names in CMIP6 correspond with one of the five shared socioeconomic pathway (SSP1-SSP5) followed by an estimate of the radiative forcing at the year 2100 between 1.9 and 8.5 Wm^{-2}. SSP1-5 are narratives that describe broad socioeconomic trends that are expected to shape the future of humanity, and are based on trends in population, urbanisation, and technological and economic growth (Riahi et al., 2017). In this work, we include: two sustainable development scenarios SSP1-1.9 and SSP1-2.6; the intermediate emissions scenario, SSP2-4.5, which has a medium radiative forcing by the end of the century; the regional rivalry scenario, SSP3-7.0, which pushes global issues into the background; and the enhanced fossil fuel development, SSP5-8.5, which has extremely high fossil fuel deployment and atmospheric CO_2 concentration (O'Neill et al., 2016; Riahi et al., 2017).

1.2 Climate Sensitivity

Given the same rise in atmospheric CO_2 concentration, each ESM will warm to a different temperature due to the structural and parametric differences between models. The Equilibrium Climate Sensitivity (ECS) is defined as the global mean near-surface air temperature rise in °C in response to a doubling of the atmospheric CO_2 concentration once the model has reached equilibrium. The 5-95% confidence range of ECS is between 2 °C and 5 °C, the likely ECS range is 2.5 - 4 °C, and the most likely value is 3 °C (Arias et al., 2021, TS6). In ESMs, the spread in the sensitivity to CO_2 between models is one of the causes

of uncertainty in the timing of when projections reach certain warming levels. Similarly, the uncertainty in the "allowable emissions" that would keep global temperature rise within policy targets are also impacted (United Nations Treaty Collection, 2015). This uncertainty is exacerbated in CMIP6 as it has a broader range of ECS values than previous generations and several CMIP6 models are outside the likely ECS range (Hausfather et al., 2022). Uncertainties in cloud feedbacks have been identified as the main cause of the large ECS range in CMIP6 (Ceppi and Nowack, 2021).

1.3 Global Warming Levels

Climate change policy has a tendency to focus on the climate at specific target years, such as 2050 or 2100 (United Nations Treaty Collection, 2015; IPCC, 2021a). However, due to the diversity of ECS values in CMIP6, the ensemble will project a wide range of warming rates and surface temperatures at a given point in time. This wide range of behaviours has knock-on effects on climate feedbacks and may inhibit the realism and representativeness of the ensemble's multi-model mean (Hausfather et al., 2022; Swaminathan et al., 2022). On the other hand, this more comprehensive range of responses is valuable in exploring carbon-climate processes that are of direct relevance to policy. Instead of specific target years, we focus on three specific Global Warming Levels (GWL). These are 2 °C, 3 °C or 4 °C of warming relative to the pre-industrial period. They allow us to generate policy relevant assessments while exploiting the full ensemble of CMIP6 models. Not only does the GWL methodology mirror the policy discourse surrounding the policy targets, it is also largely independent of the choice of future emissions scenario as the world largely looks the same at 2 °C, no matter how we get there (Hausfather et al., 2022). In addition, GWL bypasses the need to select or weight CMIP6 models as each model provides distinct and relevant information, so the full CMIP6 ensemble can be used (Hausfather et al., 2022). The three GWLs were chosen because the 2 °C GWL is a key target set in the 2015 Paris Agreement and thought to be a threshold for potentially dangerous climate change (United Nations Treaty Collection, 2015). The 3 °C GWL is the warming level that current nationally determined emission policies will realise for the year 2100 assuming a median climate sensitivity (United Nations Environment Programme, 2019). Finally, the 4 °C GWL is a low likelihood but high impact outcome if climate sensitivity is higher than median values or emission reductions and climate policy break down (World Bank, 2012).

This is the first work that presents the carbon allocation using the GWL framework. Previous analyses project carbon allocation at an arbitrary point in time using the mean of a set of models with widely different warming rates and sensitivities (IPCC, 2021a; Canadell et al., 2021). When compared against projections at specific points in time, our results are less influenced by the overall climate sensitivity of the ensemble and may be more relevant to policymakers.

2 Methods

2.1 Carbon allocation calculation

We calculate the carbon allocation for the land, ocean and atmospheric reservoirs separately. The land carbon sink, S_{Land}, is derived from two other fields: the net biome production, *NBP*, and global total land use emissions, *LUE*. The *NBP* is a

diagnostic variable calculated by the models and it is defined as positive for fluxes into the land carbon store in CMIP6 (Jones et al., 2016). S_{Land} is the activity of the vegetation, which is the combined carbon flux of all natural sources, including photosynthesis, respiration, wildfire and other sinks and sources. These natural fluxes and therefore the carbon sinks are altered by anthropogenic carbon emissions into the atmosphere, for example from fossil fuel combustion. S_{Land} is positive in the direction of a sink into the land from the atmosphere, but it does not the effects of anthropogenic land-use change. The *LUE* are anthropogenic carbon sinks and sources, including deforestation, land management, reforestation and others (Lawrence et al., 2016). *LUE* is positive into the atmosphere. *NBP* is a diagnostic that combines both S_{land} and *LUE*. *NBP* is positive into the land, so for these sign conventions, *NBP* $= S_{Land} -$ *LUE*, and represents the net exchange between land and atmosphere including anthropogenic emissions relating to land use change. The directions for these fluxes that are taken as positive are indicated in Fig. 1. To diagnose only the S_{Land} component, it is therefore necessary to add back in the *LUE* to *NBP*. As such, S_{Land} is here computed as the sum of the global total net biome production and the global total land use emissions:

$$S_{Land} = NBP + LUE \tag{1}$$

ESMs produce *NBP* as a diagnostic field in the *nbp* dataset, but this is actually their total carbon change in the land. It is not possible to directly isolate the *LUE* for each model and ensemble member in CMIP6 simulations, and the *LUE* value are calculated from prescribed land use scenarios and are common across all models and all ensemble members following Liddicoat et al. (2021). A more accurate method of determining the *LUE* would be to calculate the difference in net biosphere production between a pair of simulations, one with land use changing over time, and the other with fixed land use (Pongratz et al., 2014; Liddicoat et al., 2021). However, these simulation pairs exist only for a limited subset of models and scenarios as part of the Land Use Model Inter-comparison Project, LUMIP (Lawrence et al., 2016). In practice, we calculated the global total net biome production as the cumulative sum along the time axis of the land surface *NBP* multiplied by the cell surface area then summed with the annual *LUE* value from Liddicoat et al. (2021).

The ocean component of the carbon allocation, S_{Ocean}, is the total global sum of the air sea flux of CO_2. We calculated this as the sum of the air-sea flux of CO_2 multiplied by the ocean area of each cell, expressed as a cumulative sum of the annual totals. Like the land surface, the ocean can be both a sink and a source of CO_2.

In the atmosphere, the global mean CO_2 concentration is provided in the scenario forcing from ScenarioMIP in units of parts per million (ppm). The total mass of the carbon in atmospheric CO_2, C_{Atmos}, is calculated by multiplying the change in concentration relative to the 1850 value in ppm by a constant factor. This conversion factor is 2.13 PgC per ppm change in CO_2 concentration (Myers, 1983). No matter how much carbon the land and ocean components absorb from the atmosphere, the atmospheric concentration of CO_2 will always strictly follow the prescribed atmospheric CO_2 concentrations of the forcing scenario. This means that anthropogenic emissions can be estimated for each model (Jones et al., 2013). The total anthropogenic carbon, C_{Total}, is the sum of the total carbon in the atmospheric CO_2, C_{Atmos} and the cumulative global total CO_2 flux into the sea, S_{Ocean}, and the land sink, S_{Land}:

$$C_{Total} = C_{Atmos} + S_{Ocean} + S_{Land} \tag{2}$$

2.2 Included Models

This analysis used all CMIP6 ESMs for which the following three variables were available as monthly averages over the time period 1850-2100: the near-surface atmospheric temperature (*tas*), the net biome productivity (*nbp*) and the air to sea flux of CO_2 (*fgco2*). We limited each model to only the first ten ensemble members for each scenario, and required at least one historical and future scenario pair for each ensemble member. The grid cell area was also required for the ocean (*areacello*), and for land and atmosphere (*areacella*) grids. We excluded the entire ensemble member if any variables were absent, the time series was incomplete, or the data could not be made compliant with CMIP6 standards.

In CMIP6, modelling centres may contribute more than one ensemble member for each scenario to the Earth System Grid Federation (ESGF). For instance, the UKESM1-0-LL model produced 19 different variants for the historical experiment, each using slightly different initial conditions drawn from the pre-industrial control (piControl) simulation (Sellar et al., 2020). This generates an ensemble of variants which samples a wide range of the unforced variability simulated by the model. By spanning the range of internal variability, the mean of a single model ensemble can give a more robust estimate of its forced climate change response.

Each modelling centre has flexibility on which scenarios they simulate and how many ensemble members are generated for each scenario. This means that there is wide variation in the number of ensemble members between models. To balance models with large ensembles against models with small ensembles, we used a "one model - one vote" weighting scheme. This ensured that each model was given equal weight in the final multi-model mean. In practice, each ensemble member of a given model was weighted inversely proportional to the number of ensemble members that the model contributed. For reasons described in Sect. 1.3, we did not weight the results regarding the model quality, sensitivity or historical performance.

Table 1 lists the contributing models, the number of ensemble members for each scenario, and each model's equilibrium climate sensitivity (ECS). The ECS plays a first order role in how rapidly a given model reaches a given GWL for a given CO_2 pathway. For most models, we took the ECS value from Zelinka et al. (2020). For the models whose ECS was not included in Zelinka et al. (2020), we use the following ECS values: ACCESS-ESM1-5 from Ziehn et al. (2020), CMCC-ESM2 from Lovato et al. (2022), EC-Earth3-CC from Hausfather et al. (2022), GFDL-ESM4 from Dunne et al. (2020), and MPI-ESM1-2-LR from Mauritsen et al. (2019). No ECS value was available for the CanESM5-CanOE model as it did not provide the abrupt $4xCO_2$ experiment required to calculate ECS using the Gregory method (Gregory et al., 2004; Christian et al., 2022). However, it only differs from CanESM5 by the addition of a marine biogeochemistry component model (Swart et al., 2019; Christian et al., 2022). We follow the method used elsewhere (Hausfather et al., 2022; Scafetta, 2022), and substitute CanESM5's ECS value for CanESM5-CanOE. Other ECS datasets also exist, see for instance: Flynn and Mauritsen (2020); Meehl et al. (2020); Weijer et al. (2020); Hausfather et al. (2022), and only differ within 0.1 °C from the values used in this study. All ECS values included here use the Gregory et al. (2004) method, however, the value of ECS for any given model is sensitive to the method that was used to derive it. See for instance Table 4 of Boucher et al. (2020), where ECS for the same model may vary by more than 1 °C depending on the methodology.

In its last row, Table 1 shows the ensemble mean ECS of the contributing models for each scenario. Following the "one-model one-vote" scheme, the "weighted ECS" only takes into account the presence or absence of models, not the number of contributing ensemble members. The spread of weighted ECS values between scenarios is small, ranging from 3.96 for SSP1-1.9 to 4.17 for SSP5-8.5. Five out of six of these ensemble means sit above the likely ECS range of 2.5 - 4 °C, and four of the individual models are outside the 5-95% confidence band, 2 - 5°C (Sherwood et al., 2020; Arias et al., 2021).

As in other CMIP ensemble studies, we attempt to maximise the number of models in this work in order to improve robustness (Flynn and Mauritsen, 2020; Meehl et al., 2020; Weijer et al., 2020; Hausfather et al., 2022). This means that we allow all available candidates, even pairs of sibling models: there are two CESM2 models and two CanESM5 models in the ensemble. CESM2-WACCM6 is configured identically to CESM2, except that it has expanded aerosol chemistry and uses 70 vertical levels and its model top is at 4.5×10^{-6} hPa (approximately 130 km), instead of CESM2's 32 vertical levels and a model top at 2.26 hPa (approximately 40 km) (Danabasoglu et al., 2020). The CanESM5-CanOE model differs from CanESM5 by the addition of a more complex marine biogeochemistry component (Christian et al., 2022).

In addition to sibling models, the same individual component models are used by several modelling centres. For instance, the NEMO ocean circulation model forms the marine circulation component model of six of the ESMs used here (Heuzé, 2021). While the ESMs use differing versions of NEMO with different configurations and settings, these models can not be treated as statistically independent. However, it is beyond the scope of this work to develop or apply a method to weight models such that the multi-model mean is statistically robust, for instance in Brunner et al. (2020).

2.3 Global warming level calculation

We calculated the global warming level following the methods of Swaminathan et al. (2022). The global mean atmospheric surface temperature is calculated for each model, scenario and ensemble member. The anomaly is the difference from the mean of the period 1850-1900 from the relevant historical ensemble member. This temperature time series is then smoothed by taking the mean of a window with a width of 21 years, i.e. 10 years either side of the central year. The first year that the smoothed global mean surface temperature anomaly exceeds the global warming level is the GWL exceedance year (see Fig. 1 of Swaminathan et al. (2022)). Due to the 21 year window and simulations ending in 2100, the last possible GWL exceedance year is 2090.

We calculate the multi-model mean for each of the variables using the "one model - one vote" scheme described above. We also determine the multi-model mean GWLs and their timings from the multi-model mean temperature, instead of taking the weighted mean of the individual ensemble members GWLs timings. This method ensures that the multi-model mean is more representative of the overall ensemble, instead of being biased towards only those models that reach the GWL.

We used the ESMValTool toolkit to perform the analysis. ESMValTool is built to facilitate the evaluation and inter-comparison of CMIP datasets by providing a set of modular and flexible tools (Righi et al., 2020). These tools include quick ways to standardise, slice, re-grid, and apply statistical operators to datasets. In our case, we used the `annual_statistics` preprocessor to calculate the annual mean, the `mask_landsea` preprocessor to mask the land or ocean areas, and the

Table 1. A list of the models, the number of contributing ensemble members for each scenario, the model ECS, and the weighted mean ECS of the contributing models. The weighted ECS row shows how the model occupancy affects the mean ECS of the ensemble for each scenario. The presence or absence of models impacts the weighted ECS, but not the number of contributing ensemble members.

Model	Historical	SSP1-1.9	SSP1-2.6	SSP2-4.5	SSP3-7.0	SSP5-8.5	ECS
ACCESS-ESM1-5	3		2	3	2	1	3.87
CESM2	3		3	3	3	3	5.15
CESM2-WACCM	3		1	3	1	3	4.68
CMCC-ESM2	1			1			3.57
CanESM5	10	10	10	10	10	10	5.64
CanESM5-CanOE	2		2	2	2		5.64
EC-Earth3-CC	8			8		1	4.23
GFDL-ESM4	1	1	1	1	1	1	2.7
IPSL-CM6A-LR	12	5	3	6	10	5	4.56
MIROC-ES2L	5	5	5	5	5	5	2.66
MPI-ESM1-2-LR	5	5	5	5	5	5	2.83
NorESM2-LM	2		1	2	1		2.56
UKESM1-0-LL	10	5	10	10	10	5	5.36
Total number of Ensembles	65	31	43	59	50	39	
Total number of Models	13	6	11	13	11	10	
Weighted ECS	4.11	3.96	4.15	4.11	4.15	4.17	

`area_statistics` preprocessor to calculate the area weighted global mean. ESMValTool is hosted on GitHub, and we have made available all of the code used in the study (see Code and data availability section).

3 Results

3.1 Multi-model mean carbon allocation

The total multi-model mean carbon allocation for each scenario at the year 2100 and for each of the three GWLs is shown in Fig. 2. The top pane shows the carbon allocation at the year 2100. At 2100, the higher emission scenarios have greater total carbon allocations and more of that carbon is allocated to the atmosphere, relative to the lower emission scenarios. At the year 2100, more carbon is allocated to the ocean than the land in SSP5-8.5, SSP3-7.0 and SSP2-4.5, while more carbon is allocated to the land than the ocean in SSP1-1.9 and SSP1-2.6. This reproduces the results discussed earlier from IPCC (2021b) Fig. SPM7.

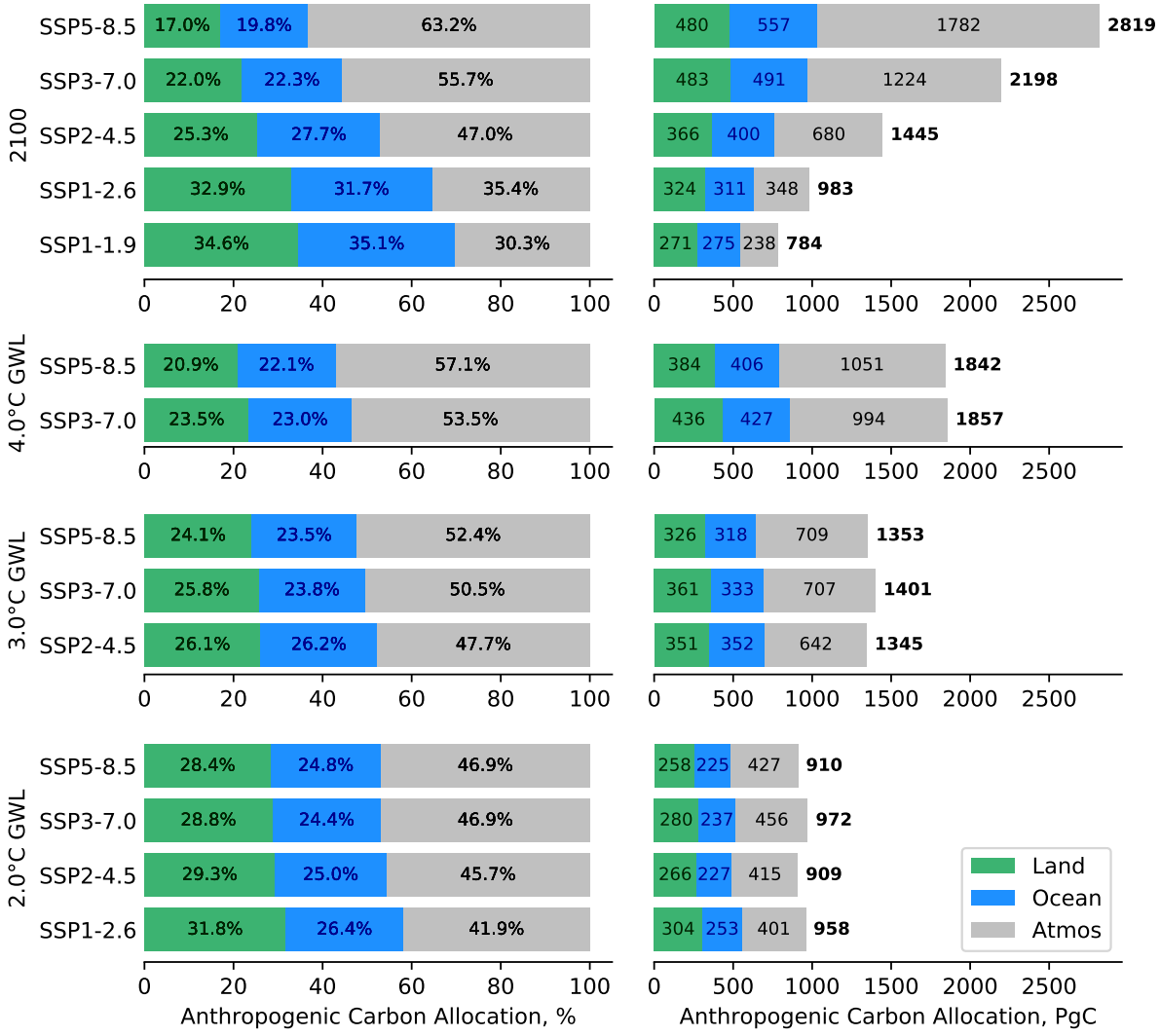

Figure 2. Carbon allocation for the multi-model mean for each scenario for the year 2100 and the three GWLs. The green, blue and grey areas represent the land, ocean and atmospheric carbon allocations. The left side shows the percentage allocation, and the right side shows the totals in PgC. The total values are shown in bold to the right of the bars. These values are rounded to the nearest 0.1% or the nearest integer PgC, so the three values may not add exactly to 100% or the total.

240 The lower three panes of Fig. 2 show the carbon allocation at each GWL. In all cases, the variability between scenarios within a single GWL is significantly less than the variability between scenarios at the year 2100 in the top pane. However, the variability within the same GWL is still significant in absolute terms. For instance, the multi-model mean total carbon allocation for the 2 °C GWL ranges from 909 PgC in SSP2-4.5 to 972 PgC in SSP3-7.0 (a range of 63 PgC). At the 3 °C GWL, the range is 56 PgC and at 4 °C GWL, the range is 15 PgC. When compared against the annual total emissions estimate, 9.4

$\pm$ 0.5 PgC yr^{-1} (Le Quéré et al., 2018), these differences between scenarios represent several years' worth of the global total anthropogenic emissions.

In the land surface, the multi-model means have a range of 46 PgC, 35 PgC, and 52 PgC between scenarios for the 2 °C, 3 °C, 4 °C GWLs respectively. The recent annual terrestrial carbon sink was 3.2 $\pm$ 0.8 PgC yr^{-1} (Le Quéré et al., 2018), so the difference between scenarios is equivalent to at least a decade's worth of current carbon absorption by the land surface.

The multi-model means of the ocean flux have a range of 28 PgC, 34 PgC, and 21 PgC between scenarios for the 2 °C, 3 °C, 4 °C GWLs respectively. This reflects the previous result that the carbon allocation to the land surface is more variable than the ocean, as the land values have wider ranges. The recent annual ocean carbon sink was 2.4 $\pm$ 0.5 PgC yr^{-1} (Le Quéré et al., 2018). Similarly to the land case described above, the difference between scenarios is equivalent to approximately one decade worth of the current ocean carbon absorption.

In the left hand side of Fig.2, the higher CO_2 concentration scenarios have a larger atmospheric fraction than lower CO_2 concentration scenarios at the same GWL. For instance, the atmospheric fraction is 46% in SSP5-8.5 and 42% SSP1-2.6 at the 2 °C GWL, and the atmospheric fraction is 51.2% in SSP5-8.5 and 47.4% SSP2-4.5 at the 3 °C GWL.

Figure 2 only shows the multi-model means, not single models; so the multi-model means that do not reach the GWL are not included in this figure. Table 1 shows that there are six models contributing to the SSP1-1.9 scenario in this analysis, yet the multi-model mean does not reach the 2 °C GWL here. Similarly, there are 11 SSP1-2.6 models, but the multi-model mean does not reach the 3 °C GWLs before the year 2100, nor does the mean of the 13 SSP2-4.5 models reach 4 °C of warming.

3.2 Carbon allocation time series

The CMIP6 multi-model mean carbon allocation time series is shown in Fig. 3. The top left pair shows the development over the historical period and the other five pairs show the projections. We include all data cumulatively from the year 1850, and all the cumulative carbon panes share the same y-axis range. The timing of each of the multi-model mean GWLs are marked as vertical lines.

In the historical pane of Fig. 3, the fractional atmospheric carbon starts to grow in the second half of the 20^{th} century, as the land fraction declines and the ocean fraction increases. However, all three reservoirs increase in absolute terms over the entire historical period. By the end of the historical period, the land and ocean match the observational records of Raupach et al. (2014) and Watson et al. (2020) reasonably well, shown as dashed horizontal lines. In future scenarios, the GWL threshold year occurs sooner in higher concentration scenarios than in lower concentrations scenarios. In all scenarios, the total anthropogenic carbon rises until at least the year 2050. In the two SSP1 scenarios, the total carbon starts to fall after this point, while it continues to grow in the other projections.

The fraction of carbon that is absorbed by the combined land and ocean reservoirs rises in the two SSP1 scenarios, remains approximately constant in SSP2-4.5 after 2050, and declines in the SSP3-7.0 and SSP5-8.5 scenarios. The time series at the year 2100 closely match the IPCC atmospheric fraction projections for the year 2100 (IPCC, 2021b, Fig. SPM7), shown in Fig. 3 as a short horizontal line at the end of the period. This corroboration of existing results allows an increased confidence that our methodology is appropriate.

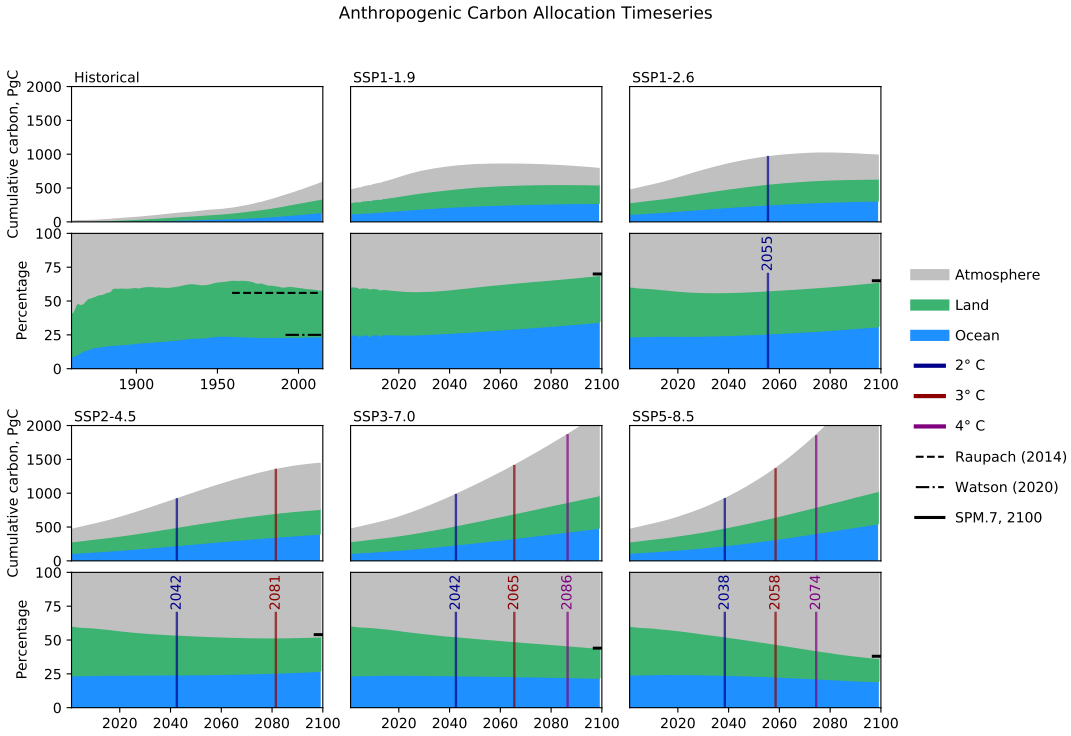

Figure 3. Multi-model mean carbon allocation time series for the historical period and each scenario. Each scenario includes a pair of panes: the top pane of each pair shows the total allocation in PgC, and the bottom pane shows the allocation as a percentage. The historical pane includes the observational records for the land and ocean fractions, from Raupach et al. (2014) & Watson et al. (2020), and the length of the lines represent the time over which the data was collected for these two observational datasets. The grey area is the cumulative anthropogenic carbon in the atmosphere, and the blue and green represent the fraction in the ocean and in the land, respectively. The SPM7 lines at the year 2100 indicate the atmospheric fraction projections from the IPCC AR6 WG1 summary for policymakers figure 7, IPCC (2021b).

3.3 Multi-model ensemble carbon allocation

Figure 4 shows the carbon allocation at each GWL as a percentage (left) and in terms of the total carbon for each model (right). For each scenario and each GWL, the models are ordered by their ECS as shown in Table 1. The lower ECS models are at the top and higher ECS models are at the bottom of each section. The lower sensitivity models take longer to reach the same warming level and have more total emissions than the higher sensitivity models. This results in the saw-tooth pattern on the right of this figure.

There is a significant variability between individual models in the total cumulative carbon allocated between scenarios at each GWL. For instance, the total carbon change at 2 °C ranges from 615 PgC (CanESM5-CanOE SSP3-7.0) to 1521 PgC (NorESM2-LM SSP3-7.0). This range of behaviours between models is very large and the difference between these two

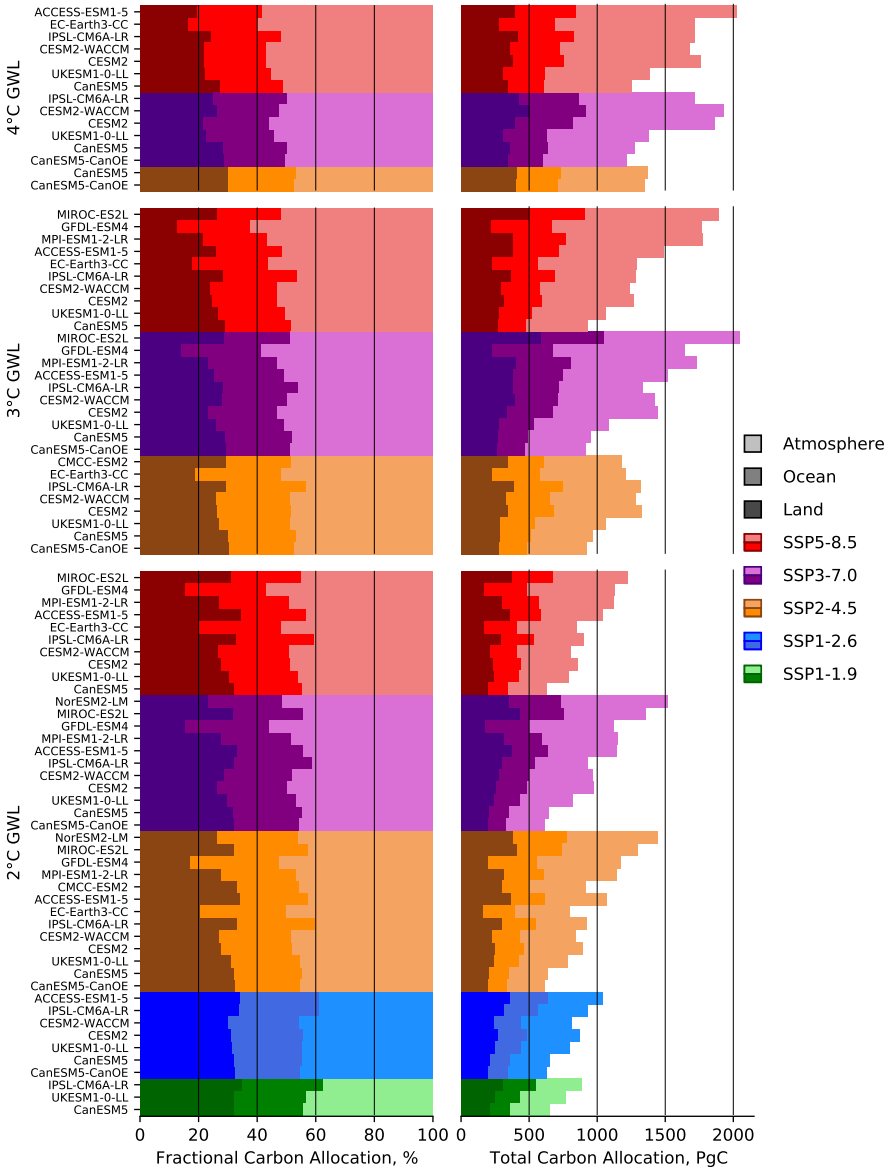

Figure 4. Global total carbon allocation for each level of warming for individual models. The left side shows the allocation as a percentage and the right side shows the total value in PgC. Each colour palette represents a different scenario, with SSP1-1.9 in greens, SSP1-2.6 in blues, SSP2-4.5 in oranges, SSP3-7.0 in purples and SSP5-8.5 in reds. The darkest shade denotes the land, the middle shade is the ocean and the lightest shade is the atmosphere. Within a given GWL and scenario, the models are ordered by their ECS, with less sensitive models at the top and more sensitive models at the bottom.

extremes is equivalent to a century's worth of current global emissions, ie 100 years of 9.4 ± 0.5 PgC yr^{-1} (Le Quéré et al., 2018).

Proportionally large ranges can also be seen in the land, ocean and atmospheric carbon sinks in Fig. 4. For instance, at the 2 °C GWL, the land has absorbed between 164 PgC (EC-Earth3-CC SSP2-4.5) and 432 PgC (MIROC-ES2L SSP3-7.0). Similarly, at the 2 °C GWL, the ocean has absorbed between 137 PgC (CanESM5-CanOE SSP3-7.0) and 401 PgC (NorESM2-LM SSP2-4.5). These ranges are equivalent to several decades worth of current global emissions, or approximately a century of the current annual rates of land or ocean carbon absorption. Almost all of the minimum and maximum values described here occur in the SSP3-7.0 scenario, for reasons described below in Sect. 4.2.

The left side of this figure shows several key results related to how carbon is allocated as a percentage of the total between models. At a given GWL, higher emission scenarios have a higher atmospheric fraction, a lower land fraction, and a relatively consistent ocean fraction. Warmer GWLs have larger atmospheric fractions, lower land fractions, and consistent ocean fractions than cooler GWLs.

3.4 Carbon allocation and ECS

The data from Fig. 4 is re-framed in fig 5 as a series of scatter plots. For each group of data, the line of best fit is calculated and the absolute value of the fitting error (Err, the standard error of the estimated gradient under the assumption of residual normality) over the slope (M) is shown in the legend, as Err/M. This value indicates whether the slope crosses the origin within the 95% confidence limit (Err/M < 1) or not (Err/M > 1). While the value always appears in the legend, the line of best fit is only shown when Err/M < 1. All groups with three models or fewer that reach the GWL were excluded as there were not enough data points to draw meaningful conclusions.

GWL year, total carbon change and the individual total carbon allocation fractions are inversely correlated to ECS. The GWL threshold year and the total carbon allocations both have all absolute Err/M values lower than unity and as such both are related to ECS. The total carbon change in both the ocean and the atmosphere are linked to ECS, as their Err/M are smaller than 1. However, the correlations between carbon allocation fraction of the ocean or the atmosphere and ECS are not statistically significant. For land, both the total carbon sink and the allocation fraction are not consistently correlated to ECS at all GWLs.

In addition to the GWL data, the values for the target year 2100 are shown in Fig. 5. The Err/M for the target year 2100 is greater than unity in the total carbon, the atmospheric carbon fraction, and both land columns, indicating a poor fit to a straight line. This indicates that ECS is not correlated to these data in target year analysis. Elsewhere, when the Err/M of the target year 2100 is less than one, it is often close to unity or larger than the Err/M of the fits to the GWL data. This indicates that ECS is often less correlated to these data in target year analysis than the GWL values. The GWL method allows us to characterise the impact of ECS, while the target year method obscures its influence.

4 Discussion

We present an analysis of the carbon allocation in the Earth System for an ensemble of CMIP6 simulations at the 2, 3 and 4 °C global warming levels. We find that through using the GWL method instead of focusing on a specific target year, we can provide estimates of the behaviour of the carbon cycle that may be more useful and relevant to policymakers. In Fig. 2, the

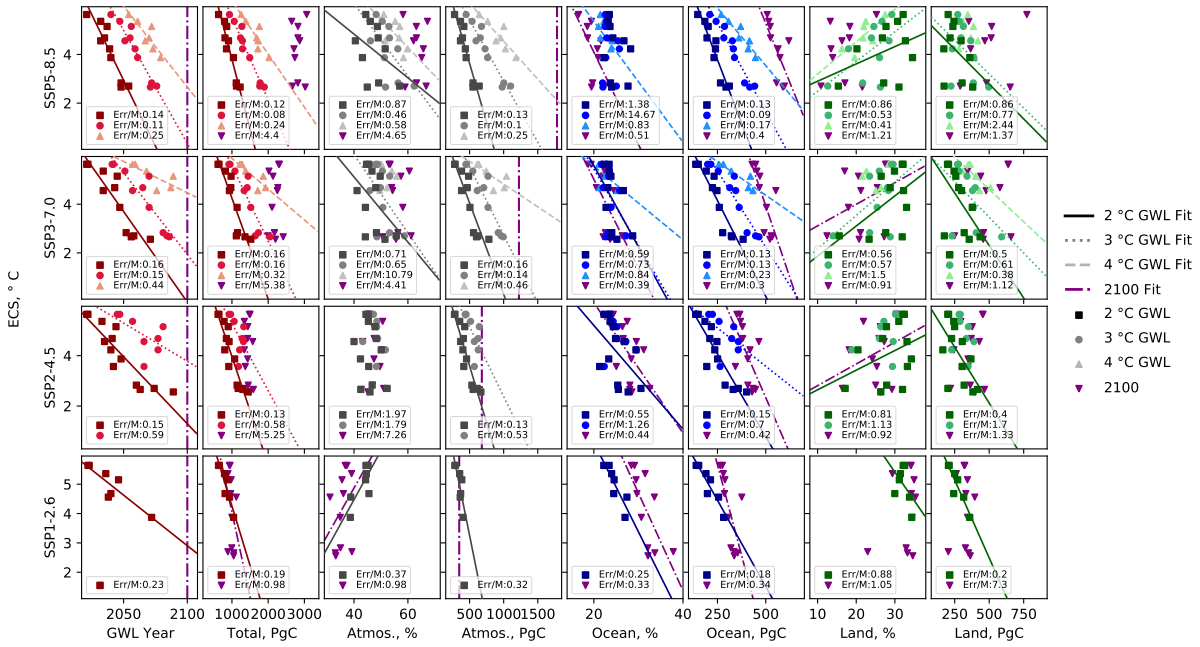

Figure 5. The GWL and target year 2100 carbon allocation scatter plot matrix. Each row represents a different scenario, and each column is a different data field, including the year, the total carbon allocated, the carbon allocation for each domain and the fractional carbon allocation to each domain. The y-axis is the model's ECS, and each point is a different GWL, where the squares are the 2° GWL, the circles are the 3° GWL, and the triangles are the 4° GWL. In all cases, the darkest colours correspond to the 2° GWL, the middle colours the 3° GWL, and the lightest colours the 4° GWL. The results for the target year 2100 are also shown in purple downward-pointing triangles. The absolute value of the fitting error of the slope over the slope is shown in the legend as Err/M. The line of best fit is shown when $\mathrm{Err/M} < 1$. The year 2100 and the total atmospheric carbon are indicated with purple vertical dash-dot lines.

difference between a focus on a specific year and the GWL method can clearly be seen by comparing the top pane against the other three panes. At the year 2100, there are large differences between the five scenarios total carbon change, the allocation between the three reservoirs and the fractional distribution. In the lower three panes, the differences between scenarios is much smaller. However, these small differences are still significant in absolute terms, where several year's worth of global CO_2 emissions separate the scenarios at each GWL. The pathway to a given GWL is scenario-dependent in two main ways. Firstly, the rate of anthropogenic CO_2 emissions has a non-negligible impact on the atmospheric fraction because the ocean and land surface can not quickly absorb the additional carbon load. A higher rate of emission leads to a slightly greater transient warming, because fractionally more of the emitted CO_2 is still in the atmosphere. Secondly, CO_2 is the primary but not the only driver of warming. Differences between the non-CO_2 forcings play a role in the realised warming at a given point in time in these scenarios. In addition, while the composition of each scenario ensemble results in a relatively uniform set of values of the mean ECS in Table 1, the mean ECS does vary by up to 0.21 °C between scenarios. This could also account for some of

the differences seen between multi-model means in Fig. 2. Furthermore, the SSP1-1.9 ensemble has the lowest mean ECS and the SSP5-8.5 ensemble has the highest mean ECS, which may exaggerate the differences between their multi-model means.

The GWL methodology allows a focused analysis on the small and subtle differences between scenarios. For instance in Canadell et al. (2021), Fig. 5.31 shows the cumulative carbon emissions against global mean temperature change for several projections. In that figure, all five projections show a strong correlation between CO_2 emissions and warming, all projections overlap at the same cumulative CO_2 emissions and there are no clear differences between scenarios for the same cumulative CO_2. Using the GWL method, we are able to focus on the differences between scenarios at the same warming level and demonstrate that small differences exist between scenarios and that the pathway to a GWL matters for the carbon allocation. While these differences in carbon allocation may only be visible under the zoomed-in focus of a GWL analysis, the differences between scenarios are consistent with previous studies and are likely due to differences in non-CO_2 forcing. However, it is beyond the scope of this work to quantify the non-CO_2 effect as in Smith et al. (2020).

On the left side of Fig. 2, the fraction of carbon that remains in the atmosphere is linked with the choice of scenario. The higher emission scenarios have higher atmospheric fractions at the same warming level. The likely mechanism is that scenarios with higher carbon concentrations simply reach the global warming levels sooner, and have proportionally less carbon allocated to the ocean and land surface at that time. The ocean and the land had not caught up with the emissions or the warming associated with that CO_2 concentration. This implies that the carbon allocation between the three major sinks is likely impacted by the rate of warming at the GWL and there may be some delay between CO_2 emissions and the equilibrium CO_2 atmospheric fraction, as the excess CO_2 is slowly absorbed by the terrestrial and oceanic sinks.

In the land surface at the 4 °C GWL, the multi-model mean land vegetation carbon increases by 384 and 436 PgC relative to 1850 in SSP5-8.5 and SSP3-7.0 respectively, as shown in Fig. 2. In CMIP5, the range relative to the years 1971-1999 was 52–477 PgC with a mean of 224 PgC, and was attributed mainly to CO_2 fertilisation of photosynthesis (Friend et al., 2014). While our CMIP6 multi-model mean is compatible with Friend et al. (2014), we do not see any individual model with only 52 PgC carbon allocated to the land at the 4 ° C GWL in fig 4. This absence is more likely to be attributed to the difference in the anomaly period (1850 vs 1971), rather than due to the significant changes between CMIP5 and CMIP6 land surface models. VISIT is the land component model that contributed the minimum value of 52 PgC in Friend's CMIP5 analysis, and VISIT is part of the MIROC-ES2L ESM in CMIP6 (Hajima et al., 2020). However, MIROC-ES2L did not reach the 4 °C GWL in any scenario presented here. In all aspects of this analysis, the land carbon allocation has a much wider range of variability than the ocean. This reflects the significant challenge and uncertainty inherent in modelling the land surface carbon cycle (Friend et al., 2014; Jiang et al., 2019).

When comparing the same model at the same GWL between scenarios, the differences between scenarios becomes even more apparent, as shown in Fig. 4. This is especially true for low ECS models. For instance, the minimum and maximum carbon allocation in the MIROC-ES2L at 2 °C GWL is 1225 PgC in SSP5-8.5 and 1361 PgC in SSP3-7.0. The difference between these two projections of the same model with the same warming level is 136 PgC. For the decade 2008–2017, the mean annual emissions were 9.4 ± 0.5 PgC yr^{-1}, so this difference alone is equivalent to approximately 14 years of the current total global emissions.

In Fig. 4, when comparing individual models between different GWLs, the highest total carbon allocation at the 2 °C GWL is 1521 PgC (NorESM2-LM SSP3-7.0). This is more carbon than several models emitted at higher GWLs: the lowest carbon emitted at 4 °C GWL was 1220 PgC for CanESM5-CanOE in the SSP3-7.0 scenario. In addition, both CanESM5 models and the UKESM1-0-LL model reached 4 °C of warming in three different scenarios with less atmospheric carbon than NorESM2-LM had when it reached the 2 °C GWL. This highlights the significant role that ECS plays in the uncertainty of warming projections. A model's sensitivity to CO_2 concentration significantly impacts its projection of the total carbon allocation at global warming levels, as well as the absolute values of the individual carbon sinks in the ocean and land.

The ocean maintains similar allocation percentages across the GWLs, but in Fig. 3 there is a small decline in ocean carbon allocation percentage at the highest CO_2 concentration scenarios towards the end of the 21^{st} century. This is likely because much of the ocean is forecast to become increasingly stratified in the coming century, which would reduce downwards mixing of CO_2 (Li et al., 2020; Muilwijk et al., 2023). This reduction in downward mixing combined by the decline in solubility with rising sea surface temperature, causes the overall absorption rate of CO_2 into the ocean to be reduced. The increase in stratification is caused by warmer surface layers, combined with gradual decline in overturning rates and overall circulation (Thibodeau et al., 2018; Li et al., 2020; Caesar et al., 2021; Sallée et al., 2021). Ocean acidification may also be playing a role in reducing the rate of the chemical transition of dissolved CO_2 and thus also slowing uptake (Zeebe, 2012). In combination, these effects act to reduce the rate that absorbed CO_2 is removed from the surface layer. In the ocean, enhanced ocean acidification has a range of effects but has been shown to decrease survival, calcification, growth, development and abundance over a broad range of marine organisms (Kroeker et al., 2013).

While the ocean fraction is more or less consistent throughout the SSP2-4.5, SSP3-7.0 and SSP5-8.5 scenarios at the GWLs, the land fraction declines over the coming century in Fig. 3, from 35% at the end of the historical period to 25.3% in SSP2-4.5, 22% in SSP3-7.0 and 17% in SSP5-8.5 at the year 2100. The land fraction is forecast to decline over the coming century in the higher CO_2 concentration scenarios, although the total land carbon allocation increases. There are several possible explanations for this slowdown of uptake. Land ecosystems have been shown to become progressively less efficient at absorbing carbon as levels of atmospheric CO_2 concentrations increase (Wang et al., 2020). The soil respiration could increase due to warming more than the carbon uptake increases due to photosynthetic uptake (Nyberg and Hovenden, 2020). Alternatively the nitrogen limitation could progressively limit photosynthetic uptake (Ågren et al., 2012). The changing climate may impact vegetation growth and photosynthetic uptake via droughts and warming, which moves plants outside the most efficient temperatures for photosynthesis. It is not clear which factors have the largest impact.

The differences in carbon allocations seen here have consequences in the real world. Global warming and higher CO_2 increases the regional and temporal variability of precipitation (Tebaldi et al., 2021). There is also the direct effect of increasing atmospheric CO_2 on radiative cooling rates. This impacts the vertical thermal structure of the atmosphere and thus tropical overturning circulations and regional precipitation. This direct effect of atmospheric CO_2 is independent of the level of warming (Bony et al., 2013). This means that models or scenarios that have a greater atmospheric fraction of CO_2 at a given GWL will be more prone to this regional response to changed atmospheric radiative cooling, stability and circulation change, than models or scenarios with a smaller CO_2 fraction in the atmosphere.

4.1 Impact of ECS

The ensemble of CMIP6 models has a wide range of ECS values, and this impacts several aspects of carbon allocation. We show that the GWL threshold year and the total carbon change are both inversely correlated with ECS. Similarly, we found that the carbon in the atmosphere and allocated to the ocean are both inversely correlated with ECS. The ECS does not appear to be consistently correlated with the total land carbon allocation or the land carbon fraction at all scenarios and GWLs. The wider uncertainty and challenging nature of land surface carbon modelling is reflected in a broader range of behaviours in land carbon models in CMIP6.

The ECS impacts the GWL threshold year, but this range is also affected by survivor bias. While we hesitate to draw conclusions from extrapolating the lines of best fit of Fig. 5, the line of best fit for the 2 °C GWL threshold year for the SSP1-2.6 scenario crosses the year 2100 at an ECS equivalent to 3.1 °C. As the likely range of ECS values could be as low as 2.5 °C, this means that a non-trivial part of the ECS-phase space could be excluded by the ScenarioMIP limit of forecasting to the year 2100. While we could extend the analysis with some longer term simulations, very few models and scenarios are available beyond the year 2100. To address this issue, the next round of ScenarioMIP in CMIP7 could extend its standard cut off beyond the year 2100. This would reduce survivor bias at 2 °C GWL and allow the inclusion of models with a low but still feasible ECS of 2.5°C.

Hausfather et al. (2022) outline a few analysis strategies for addressing the "hot model" problem in CMIP6. The first option is to use the GWL methodology as we have in this work. One of the alternative recommendations is to perform analysis of CMIP6 ensembles without the contributions of models that fall outside the likely ECS range of 2.5 - 4 °C. In our case, this would remove seven of the thirteen models from the analysis, leaving six or fewer models contributing to each scenario. This would be an unnecessarily harsh requirement as we have already demonstrated that using GWL methodology can reduce the impact of the range of ECS relative to the "target year" methodology. In addition, uncertainties in cloud feedbacks have been identified as the main cause of the large range of ECS (Ceppi and Nowack, 2021), and it is unlikely that there is direct link between a models ability to reproduce cloud feedback behaviour and its ability to reproduce the carbon allocation, as these are independently modelled systems.

We have used the terms effective climate sensitivity and equilibrium climate sensitivity interchangeably. However, they are not the same. Gjermundsen et al. (2021) compared two Earth System models, NorESM2 and CESM2, that had the same atmospheric model but different ocean components. These two models had very different EffCS values but were otherwise very similar. NorESM2's EffCS is 2.56 °C and CESM2's EffCS is 5.15 °C. In that work, they found that the greater heat storage at depth in NorESM2 delayed the Southern Ocean's surface warming and associated cloud responses, which in turn delayed the global mean surface warming. This effect appeared in the $4xCO_2$ simulation several centuries after the 150 year cutoff used to calculate ECS with the Gregory method (Gregory et al., 2004). After a sufficient number of simulated years, the same cloud feedback eventually occurs in both models, the same warming is realised, and the two models would show similar equilibrium climate sensitivities. The Gregory method for calculating the effective climate sensitivity that was used by Zelinka et al. (2020) to generate the ECS values used here does not tell the entire story for the eventually realised warming from a given cumulative

emission, because it is not fully compatible with the true equilibrium climate sensitivity. It may be possible to take this effect into account in future works, for instance, by replacing the surface atmospheric warming anomaly with some measure of the global volume-weighted mean ocean heat anomaly.

4.2 Anomalous behaviour in SSP3-7.0

The SSP3-7.0 scenario often appears to be an outlier. For instance, in figs. 2 and 4, it does not conform to the pattern of the other scenarios. In addition, SSP3-7.0 is the scenario showing the widest range of carbon allocation behaviours at both the 2 °C and 3 °C GWLs in Fig. 4. The SSP3-7.0 scenario has the highest methane concentration and air pollution precursor emissions forcing, even higher than those in SSP5-8.5 (Meinshausen et al., 2017, 2020). In the other scenarios, the methane and aerosol precursors scale approximately in proportion to the CO_2 concentration. Methane is a strong greenhouse gas and has a warming effect, but pollution precursor emissions are linked to aerosols and cloud formation, which generally have a cooling effect (Twomey, 1977; Meinshausen et al., 2017). In CMIP6, methane warming can overwhelm, be overwhelmed by, or balance with aerosol cooling and the relative strengths of these effects depend strongly on the model parameterisation choices and their relative strengths in the scenario forcing. The relative strength of the warming methane emissions and the cooling aerosol precursors determines the impact on the warming rate and hence the GWL timing. This is why the warming in SSP3-7.0 is not as tightly bound to the atmospheric CO_2 concentration as in other scenarios. Even though warming is still correlated to total cumulative emissions, SSP3 scenarios may reach the GWLs relatively earlier or later than other scenarios at the same CO_2 concentration. This effect could be investigated in detail if for instance the SSP3-8.5 or SSP5-7.0 scenarios were simulated.

The impact of different methane and aerosol precursor emissions on the climate response remains highly uncertain in CMIP6. The overall warming impact of methane is not further considered in this work as is it secondary to CO_2 warming, but it could be examined in future extensions.

4.3 Limitations and possible extensions

While the CMIP6 experiments start in 1850 from a pre-industrial control, clearly this is not the starting point for the anthropogenic impact on the land surface or the carbon cycle. The human impact on the environment began much earlier and this has implications for on-going carbon partitioning (Bronselaer et al., 2017; Le Quéré et al., 2018; Friedlingstein et al., 2022). For instance, between 1765 and 1850, atmospheric CO_2 rose by roughly 10 ppm, and accounting for this era resulted in a 4.5% change in ocean uptake in CMIP5 models (Bronselaer et al., 2017).

Similarly, the representation of dynamic vegetation, soil carbon and fire response is most likely under-sampled in this ensemble (Arora et al., 2020; Koch et al., 2021). Notably, CMIP6 models are not capturing present-day tropical forest carbon dynamics; the multi-model mean estimate of the pan-tropical carbon sink is half of the observational estimate (Koch et al., 2021). This uncertainty in the strength of carbon–concentration and carbon–climate feedbacks over land is well established (Cox et al., 2000; Friedlingstein et al., 2006; Arora et al., 2013).

The global ocean carbon inventory is also affected by the land-to-ocean carbon flux from river runoff and the carbon burial in ocean sediments, which is not represented in our ensemble (Arora et al., 2020). The flux of land carbon into the ocean

via rivers is between 0.45 $\pm$ 0.18 PgC yr^{-1} and 0.78 $\pm$ 0.41 PgC yr^{-1} and is generally not considered in ESMs (Jacobson et al., 2007; Resplandy et al., 2018; Hauck et al., 2020). Including the riverine flux of particulate and dissolved organic carbon would require models to represent both estuarine and shallow shelf processes. This would most likely require higher model resolutions and computational costs.

One of the limitations of the GWL methodology is that it focuses on the realised warming at a specific point in time. This is the transient warming, and it is unlikely that this warming includes the full effect of all cumulative CO_2 emissions. In effect, the CO_2 emissions have not yet played out to equilibrium at the GWL, and there is likely to be a continued delay in their warming effect.

Not all scenarios are expected to reach these warming thresholds before the year 2100. For instance, while it is highly likely that all SSP5-8.5 simulations will reach 2 °C of warming, it is unlikely that any SSP1-1.9 experiments will reach 4 °C of warming. On the other hand, only some of the models reach the threshold in certain combinations of scenario and GWL. For instance, three of the six SSP1-1.9 models reach the 2 °C GWL. These missing models would most likely reach the thresholds at some point after the year 2100, if allowed to run for enough additional years with positive net CO_2 emissions. Future works could potentially extend their analysis by including the long-timeline scenarios beyond the year 2100. The method that we used to populate Fig. 2 took the multi-model mean first with all models contributing equally, then used that ensemble mean to calculate the GWL threshold years. An alternative method could first calculate the GWL threshold years for individual ensemble members, then take the mean of only those that reach the threshold. However, this alternative method would implicitly include survivor bias, causing the overall weighting and conclusions to be biased towards high ECS models.

In this work, we used concentration driven scenarios instead of emission driven scenarios. Emission driven scenarios allow significantly more flexibility in the behaviour of the atmospheric carbon. In practice, this would be like adding a third degree of freedom into the total carbon allocation calculation. Although a limited set of emission driven runs exist, it was found that there are actually very few differences in simulated temperature or atmospheric CO_2 concentration between concentration driven and emission driven scenarios (Lee et al., 2021, Sec. 4.3.1.1). In any case, several key datasets required in the calculation of the land use emissions (*LUE* in Eq. 1) were not available in the emission driven experiments at the time of writing.

In Fig. 3, the multi-model mean of both SSP1 scenarios shows signs of recovery and carbon drawdown, but no datasets in this analysis drop below the 2 °C GWL threshold. In future studies, it would be interesting to examine the reversibility of carbon allocation with negative emission forcing scenarios. More generally, extension simulations beyond 2100 would be valuable for studying how patterns of carbon allocation change as emissions decline past net-zero.

In fig 5, we generated a fit to each dataset against the ECS. This fit is built on the assumption that these behaviours are linear and that the straight line fit is a reasonable approximation of their behaviour. However, as can be seen in this figure, this is not true in all cases. Several of the datasets have non-linear behaviours with regards to ECS. It may be possible to expand upon this work and generate more complex fits to these datasets to estimate the behaviour of these models within the likely ECS range of 2.5 - 4 °C.

In this work, we attempt to maximise the number of models. ScenarioMIP's flexible contributions means that each scenario's ensemble is composed of a different set of models, as shown in Table 1. This diversity results in a different mean ECS for each

scenario. We were fortunate that the range of the mean ECS values was only 0.21 °C, despite for instance SSP1-1.9 containing significantly fewer models that the other scenarios. A different set of models could conceivably result in a wider range of mean ECS values between scenarios, which would impact the warming rates at the same CO_2 concentrations, making interpretation more challenging and potentially introducing bias in the conclusions. In future investigations of CMIP multi-model means using the GWL methodology, the mean equilibrium climate sensitivity of each ensemble should be included alongside the analysis as two ensembles constituted of differing sets of models may not always be directly comparable.

5 Conclusions

Using an ensemble of CMIP6 simulations, we have quantified how the carbon allocation between Earth System components differs between scenarios after the same change in global mean surface temperature anomaly. Scenarios with higher carbon concentrations reach the global warming levels sooner, and have proportionally less carbon allocated to the ocean and land surface at that time than scenarios with lower emissions. The differences in estimated carbon emissions between scenarios vary even at the same GWL, and can be equivalent to several years' worth of global total emissions. This is a result of the GWL methodology, but our conclusions are nevertheless compatible with previous works and we do not claim to refute previous target year analyses.

A model's sensitivity to CO_2 concentration significantly affects its total carbon allocation between the atmosphere, ocean and land at all global warming levels. However, our CMIP6 ensemble contains many models that fall outside the likely ECS range of 2.5 - 4 °C. By using the GWL methodology, we can exploit the full CMIP6 ensemble and weight each model equally, without excluding the so-called "hot models". We did not find a consistent relationship between ECS and any of the fractional carbon allocations. However, we did demonstrate that ECS and total carbon allocation are related. Models with lower sensitivity to carbon reach the GWL with more carbon in the individual reservoirs and more carbon overall. This is because it takes low ECS models longer to reach the same warming level, allowing more time for carbon to accumulate in the Earth System.

In addition to the impacts of ECS and total atmospheric carbon concentration, the distinct characteristics of each scenario pathway also influences the carbon allocation. The SSP3-7.0 scenario includes both high methane-induced warming and high pollution precursors cooling, and the strength of these effects are model specific and not directly related to ECS. These environmental forcers in SSP3-7.0 can generate a very different warming response, GWL threshold year and carbon allocation than scenarios where CO_2, methane and pollution precursors all scale with historical values.

Ultimately, across all model simulations, a significant rise in global mean surface temperature is projected over the 21^{st} century. This underscores the need for an accelerating transition to low carbon technologies to reduce the risk of the worst effects of climate change.

Code and data availability. This analysis was performed using ESMValTool and the exact software tools used in this manuscript are available via zenodo: 10.5281/zenodo.8335060, version 1.1. The main ESMValTool recipe is `recipe_gwt_time_series_CMIP6_2022_all.yml`

in the `esmvaltool/recipes` directory, and the main diagnostic script is `diagnostic_gwt_timeseries.py` in the `esmvaltool/diag_scripts/ocean` directory. An up-to-date version of the base ESMValTool system is available on github: github.com/ESMValGroup which includes up to date code, documentation and tutorials. CMIP6 climate model data used in this paper was obtained from the CEDA's Earth System Federation Grid node, but is widely available elsewhere: https://esgf-node.llnl.gov/search/cmip6/

Video supplement. A video abstract for this paper is available here: path-to-be-confirmed.

Author contributions. All authors contributed to the writing, discussion, initial outline, literature survey and editorial feedback of the manuscript. LdM led the work, performed the analyses and led the writing. RS, CGJ, LdM developed the GWL analysis methods. CDJ, SL, TQ contributed to the land surface carbon calculation. JW contributed to the extraction and curation of the model data. CGJ, JB, led the UKESM1 and TerraFirma projects and working groups where this work was funded.

Competing interests. The authors are not aware of any competing interests.

Acknowledgements. LdM and DIK were supported by the UK Natural Environment Research Council through The UK Earth System Modelling Project (UKESM, grant no. NE/N017951/1). RS, RJP, TQ and RPA are funded by the UK National Centre for Earth Observation (NE/N018079/1). LdM, RS, JB, RJP, CDJ, CGJ, AY were supported by the UK Natural Environment Research Council through the TerraFIRMA: Future Impacts, Risks and Mitigation Actions in a changing Earth System project, Grant reference NE/W004895/1. CGJ acknowledges funding from the NERC National Capability UKESM grant no. NE/N017978/1 and EU Horizon 2020 project CRESCENDO, grant number: 641816. CDJ, SL and JW were supported by the Joint UK BEIS/Defra Met Office Hadley Centre Climate Programme (GA01101). CDJ was supported by the European Union's Horizon 2020 research and innovation programme under Grant Agreement No 101003536 (ESM2025 - Earth System Models for the Future). The authors would like to acknowledge use of the Centre for Environmental Data Analysis (CEDA) JASMIN computing cluster and BADC data centres in this work. The authors would also like to thank the JASMIN and ESMValTool teams for their assistance with this work. The authors would also like to acknowledge anonymous reviewer #1 and Dr. John Dunne for their patience and contributions towards the final manuscript.

References

Ågren, G. I., Wetterstedt, J. A. M., and Billberger, M. F. K.: Nutrient limitation on terrestrial plant growth – modeling the interaction between nitrogen and phosphorus, New Phytologist, 194, 953–960, https://doi.org/10.1111/j.1469-8137.2012.04116.x, 2012.

Allen, M. R., Frame, D. J., Huntingford, C., Jones, C. D., Lowe, J. A., Meinshausen, M., and Meinshausen, N.: Warming caused by cumulative carbon emissions towards the trillionth tonne, Nature, 458, 1163–1166, https://doi.org/10.1038/nature08019, 2009.

Arias, P., Bellouin, N., Coppola, E., Jones, R., Krinner, G., Marotzke, J., Naik, V., Palmer, M., Plattner, G.-K., Rogelj, J., Rojas, M., Sillmann, J., Storelvmo, T., Thorne, P., Trewin, B., Achuta Rao, K., Adhikary, B., Allan, R., Armour, K., Bala, G., Barimalala, R., Berger, S., Canadell, J., Cassou, C., Cherchi, A., Collins, W., Collins, W., Connors, S., Corti, S., Cruz, F., Dentener, F., Dereczynski, C., Di Luca, A., Diongue Niang, A., Doblas-Reyes, F., Dosio, A., Douville, H., Engelbrecht, F., Eyring, V., Fischer, E., Forster, P., Fox-Kemper, B., Fuglestvedt, J., Fyfe, J., Gillett, N., Goldfarb, L., Gorodetskaya, I., Gutierrez, J., Hamdi, R., Hawkins, E., Hewitt, H., Hope, P., Islam, A., Jones, C., Kaufman, D., Kopp, R., Kosaka, Y., Kossin, J., Krakovska, S., Lee, J.-Y., Li, J., Mauritsen, T., Maycock, T., Meinshausen, M., Min, S.-K., Monteiro, P., Ngo-Duc, T., Otto, F., Pinto, I., Pirani, A., Raghavan, K., Ranasinghe, R., Ruane, A., Ruiz, L., Sallée, J.-B., Samset, B., Sathyendranath, S., Seneviratne, S., Sörensson, A., Szopa, S., Takayabu, I., Tréguier, A.-M., van den Hurk, B., Vautard, R., von Schuckmann, K., Zaehle, S., Zhang, X., and Zickfeld, K.: Climate Change 2021: The Physical Science Basis. Contribution of Working Group I to the Sixth Assessment Report of the Intergovernmental Panel on Climate Change: Technical Summary, p. 33-144, Cambridge University Press, Cambridge, United Kingdom and New York, NY, USA, https://doi.org/10.1017/9781009157896.002, 2021.

Arora, V. K., Boer, G. J., Friedlingstein, P., Eby, M., Jones, C. D., Christian, J. R., Bonan, G., Bopp, L., Brovkin, V., Cadule, P., Hajima, T., Ilyina, T., Lindsay, K., Tjiputra, J. F., and Wu, T.: Carbon–Concentration and Carbon–Climate Feedbacks in CMIP5 Earth System Models, Journal of Climate, 26, 5289 – 5314, https://doi.org/10.1175/JCLI-D-12-00494.1, 2013.

Arora, V. K., Katavouta, A., Williams, R. G., Jones, C. D., Brovkin, V., Friedlingstein, P., Schwinger, J., Bopp, L., Boucher, O., Cadule, P., Chamberlain, M. A., Christian, J. R., Delire, C., Fisher, R. A., Hajima, T., Ilyina, T., Joetzjer, E., Kawamiya, M., Koven, C. D., Krasting, J. P., Law, R. M., Lawrence, D. M., Lenton, A., Lindsay, K., Pongratz, J., Raddatz, T., Séférian, R., Tachiiri, K., Tjiputra, J. F., Wiltshire, A., Wu, T., and Ziehn, T.: Carbon–concentration and carbon–climate feedbacks in CMIP6 models and their comparison to CMIP5 models, Biogeosciences, 17, 4173–4222, https://doi.org/10.5194/bg-17-4173-2020, 2020.

Bony, S., Bellon, G., Klocke, D., Sherwood, S., Fermepin, S., and Denvil, S.: Robust direct effect of carbon dioxide on tropical circulation and regional precipitation, Nature Geoscience, 6, 447–451, https://doi.org/10.1038/ngeo1799, 2013.

Boucher, O., Servonnat, J., Albright, A. L., Aumont, O., Balkanski, Y., Bastrikov, V., Bekki, S., Bonnet, R., Bony, S., Bopp, L., Braconnot, P., Brockmann, P., Cadule, P., Caubel, A., Cheruy, F., Codron, F., Cozic, A., Cugnet, D., D'Andrea, F., Davini, P., de Lavergne, C., Denvil, S., Deshayes, J., Devilliers, M., Ducharne, A., Dufresne, J.-L., Dupont, E., Éthé, C., Fairhead, L., Falletti, L., Flavoni, S., Foujols, M.-A., Gardoll, S., Gastineau, G., Ghattas, J., Grandpeix, J.-Y., Guenet, B., Guez, Lionel, E., Guilyardi, E., Guimberteau, M., Hauglustaine, D., Hourdin, F., Idelkadi, A., Joussaume, S., Kageyama, M., Khodri, M., Krinner, G., Lebas, N., Levavasseur, G., Lévy, C., Li, L., Lott, F., Lurton, T., Luyssaert, S., Madec, G., Madeleine, J.-B., Maignan, F., Marchand, M., Marti, O., Mellul, L., Meurdesoif, Y., Mignot, J., Musat, I., Ottlé, C., Peylin, P., Planton, Y., Polcher, J., Rio, C., Rochetin, N., Rousset, C., Sepulchre, P., Sima, A., Swingedouw, D., Thiéblemont, R., Traore, A. K., Vancoppenolle, M., Vial, J., Vialard, J., Viovy, N., and Vuichard, N.: Presentation and Evaluation of the IPSL-CM6A-LR Climate Model, Journal of Advances in Modeling Earth Systems, 12, e2019MS002 010, https://doi.org/10.1029/2019MS002010, 2020.

Bronselaer, B., Winton, M., Russell, J., Sabine, C. L., and Khatiwala, S.: Agreement of CMIP5 Simulated and Observed Ocean Anthropogenic CO_2 Uptake, Geophysical Research Letters, 44, 12,298–12,305, https://doi.org/10.1002/2017GL074435, 2017.

Brunner, L., Pendergrass, A. G., Lehner, F., Merrifield, A. L., Lorenz, R., and Knutti, R.: Reduced global warming from CMIP6 projections when weighting models by performance and independence, Earth System Dynamics, 11, 995–1012, https://doi.org/10.5194/esd-11-995-2020, 2020.

Burton, C., Kelley, D. I., Jones, C. D., Betts, R. A., Cardoso, M., and Anderson, L.: South American fires and their impacts on ecosystems increase with continued emissions, Climate Resilience and Sustainability, 1, e8, https://doi.org/10.1002/cli2.8, 2022.

Caesar, L., McCarthy, G. D., Thornalley, D. J. R., Cahill, N., and Rahmstorf, S.: Current Atlantic Meridional Overturning Circulation weakest in last millennium, Nature Geoscience, 14, 118–120, https://doi.org/10.1038/s41561-021-00699-z, 2021.

Caldeira, K. and Wickett, M. E.: Anthropogenic carbon and ocean pH, Nature, 425, 365–365, https://doi.org/10.1038/425365a, 2003.

Canadell, J., Monteiro, P., Costa, M., Cotrim da Cunha, L., Cox, P., Eliseev, A., Henson, S., Ishii, M., Jaccard, S., Koven, C., Lohila, A., Patra, P., Piao, S., Rogelj, J., Syampungani, S., Zaehle, S., and Zickfeld, K.: Global Carbon and other Biogeochemical Cycles and Feedbacks, p. 673–816, Cambridge University Press, Cambridge, United Kingdom and New York, NY, USA, https://doi.org/10.1017/9781009157896.007, 2021.

Ceppi, P. and Nowack, P.: Observational evidence that cloud feedback amplifies global warming, Proceedings of the National Academy of Sciences, 118, e2026290 118, https://doi.org/10.1073/pnas.2026290118, 2021.

Christian, J. R., Denman, K. L., Hayashida, H., Holdsworth, A. M., Lee, W. G., Riche, O. G. J., Shao, A. E., Steiner, N., and Swart, N. C.: Ocean biogeochemistry in the Canadian Earth System Model version 5.0.3: CanESM5 and CanESM5-CanOE, Geoscientific Model Development, 15, 4393–4424, https://doi.org/10.5194/gmd-15-4393-2022, 2022.

Cox, P. M., Betts, R. A., Jones, C. D., Spall, S. A., and Totterdell, I. J.: Acceleration of global warming due to carbon-cycle feedbacks in a coupled climate model, Nature, 408, 184–187, https://doi.org/10.1038/35041539, 2000.

Danabasoglu, G., Lamarque, J.-F., Bacmeister, J., Bailey, D. A., DuVivier, A. K., Edwards, J., Emmons, L. K., Fasullo, J., Garcia, R., Gettelman, A., Hannay, C., Holland, M. M., Large, W. G., Lauritzen, P. H., Lawrence, D. M., Lenaerts, J. T. M., Lindsay, K., Lipscomb, W. H., Mills, M. J., Neale, R., Oleson, K. W., Otto-Bliesner, B., Phillips, A. S., Sacks, W., Tilmes, S., van Kampenhout, L., Vertenstein, M., Bertini, A., Dennis, J., Deser, C., Fischer, C., Fox-Kemper, B., Kay, J. E., Kinnison, D., Kushner, P. J., Larson, V. E., Long, M. C., Mickelson, S., Moore, J. K., Nienhouse, E., Polvani, L., Rasch, P. J., and Strand, W. G.: The Community Earth System Model Version 2 (CESM2), Journal of Advances in Modeling Earth Systems, 12, e2019MS001 916, https://doi.org/10.1029/2019MS001916, 2020.

Dunne, J. P., Horowitz, L. W., Adcroft, A. J., Ginoux, P., Held, I. M., John, J. G., Krasting, J. P., Malyshev, S., Naik, V., Paulot, F., Shevliakova, E., Stock, C. A., Zadeh, N., Balaji, V., Blanton, C., Dunne, K. A., Dupuis, C., Durachta, J., Dussin, R., Gauthier, P. P. G., Griffies, S. M., Guo, H., Hallberg, R. W., Harrison, M., He, J., Hurlin, W., McHugh, C., Menzel, R., Milly, P. C. D., Nikonov, S., Paynter, D. J., Ploshay, J., Radhakrishnan, A., Rand, K., Reichl, B. G., Robinson, T., Schwarzkopf, D. M., Sentman, L. T., Underwood, S., Vahlenkamp, H., Winton, M., Wittenberg, A. T., Wyman, B., Zeng, Y., and Zhao, M.: The GFDL Earth System Model Version 4.1 (GFDL-ESM 4.1): Overall Coupled Model Description and Simulation Characteristics, Journal of Advances in Modeling Earth Systems, 12, e2019MS002 015, https://doi.org/10.1029/2019MS002015, 2020.

Erda, L., Wei, X., Hui, J., Yinlong, X., Yue, L., Liping, B., and Liyong, X.: Climate change impacts on crop yield and quality with CO_2 fertilization in China., Philos Trans R Soc Lond B Biol Sci., 360, 2149 – 2154, https://doi.org/doi/10.1098/rstb.2005.1743, 2005.

Eyring, V., Bony, S., Meehl, G. A., Senior, C. A., Stevens, B., Stouffer, R. J., and Taylor, K. E.: Overview of the Coupled Model Intercomparison Project Phase 6 (CMIP6) experimental design and organization, Geoscientific Model Development, 9, 1937–1958, https://doi.org/10.5194/gmd-9-1937-2016, 2016.

Flynn, C. M. and Mauritsen, T.: On the climate sensitivity and historical warming evolution in recent coupled model ensembles, Atmospheric Chemistry and Physics, 20, 7829–7842, https://doi.org/10.5194/acp-20-7829-2020, 2020.

Friedlingstein, P., Cox, P., Betts, R., Bopp, L., von Bloh, W., Brovkin, V., Cadule, P., Doney, S., Eby, M., Fung, I., Bala, G., John, J., Jones, C., Joos, F., Kato, T., Kawamiya, M., Knorr, W., Lindsay, K., Matthews, H. D., Raddatz, T., Rayner, P., Reick, C., Roeckner, E., Schnitzler, K.-G., Schnur, R., Strassmann, K., Weaver, A. J., Yoshikawa, C., and Zeng, N.: Climate–Carbon Cycle Feedback Analysis: Results from the C4MIP Model Intercomparison, Journal of Climate, 19, 3337 – 3353, https://doi.org/10.1175/JCLI3800.1, 2006.

Friedlingstein, P., O'Sullivan, M., Jones, M., Andrew, R., Gregor, L., Hauck, J., Le Quéré, C., Luijkx, I., Olsen, A., Peters, G., Peters, W., Pongratz, J., Schwingshackl, C., Sitch, S., Canadell, J., Ciais, P., Jackson, R., Alin, S., Alkama, R., and Zheng, B.: Global Carbon Budget 2022, Earth System Science Data, 14, 4811–4900, https://doi.org/10.5194/essd-14-4811-2022, 2022.

Friend, A. D., Lucht, W., Rademacher, T. T., Keribin, R., Betts, R., Cadule, P., Ciais, P., Clark, D. B., Dankers, R., Falloon, P. D., Ito, A., Kahana, R., Kleidon, A., Lomas, M. R., Nishina, K., Ostberg, S., Pavlick, R., Peylin, P., Schaphoff, S., Vuichard, N., Warszawski, L., Wiltshire, A., and Woodward, F. I.: Carbon residence time dominates uncertainty in terrestrial vegetation responses to future climate and atmospheric CO_2, Proceedings of the National Academy of Sciences, 111, 3280–3285, https://doi.org/10.1073/pnas.1222477110, 2014.

Gjermundsen, A., Nummelin, A., Olivié, D., Bentsen, M., Seland, Ø., and Schulz, M.: Shutdown of Southern Ocean convection controls long-term greenhouse gas-induced warming, Nature Geoscience, 14, 724–731, https://doi.org/10.1038/s41561-021-00825-x, 2021.

Gregory, J. M., Ingram, W. J., Palmer, M. A., Jones, G. S., Stott, P. A., Thorpe, R. B., Lowe, J. A., Johns, T. C., and Williams, K. D.: A new method for diagnosing radiative forcing and climate sensitivity, Geophysical Research Letters, 31, https://doi.org/10.1029/2003GL018747, 2004.

Hajima, T., Watanabe, M., Yamamoto, A., Tatebe, H., Noguchi, M. A., Abe, M., Ohgaito, R., Ito, A., Yamazaki, D., Okajima, H., Ito, A., Takata, K., Ogochi, K., Watanabe, S., and Kawamiya, M.: Development of the MIROC-ES2L Earth system model and the evaluation of biogeochemical processes and feedbacks, Geoscientific Model Development, 13, 2197–2244, https://doi.org/10.5194/gmd-13-2197-2020, 2020.

Hansen, J., Johnson, D., Lacis, A., Lebedeff, S., Lee, P., Rind, D., and Russell, G.: Climate Impact of Increasing Atmospheric Carbon Dioxide, Science, 213, 957–966, https://doi.org/10.1126/science.213.4511.957, 1981.

Hauck, J., Zeising, M., Le Quéré, C., Gruber, N., Bakker, D. C. E., Bopp, L., Chau, T. T. T., G urses, O., Ilyina, T., Landschützer, P., Lenton, A., Resplandy, L., Rödenbeck, C., Schwinger, J., and Séférian, R.: Consistency and Challenges in the Ocean Carbon Sink Estimate for the Global Carbon Budget, Frontiers in Marine Science, 7, https://doi.org/10.3389/fmars.2020.571720, 2020.

Hausfather, Z., Marvel, K., Schmidt, G. A., Nielsen-Gammon, J. W., and Zelinka, M.: Climate simulations: Recognize the 'hot model' problem, Nature, 605, 26–29, https://doi.org/10.1038/d41586-022-01192-2, 2022.

Heuzé, C.: Antarctic Bottom Water and North Atlantic Deep Water in CMIP6 models, Ocean Science, 17, 59–90, https://doi.org/10.5194/os-17-59-2021, 2021.

Hilmi, N., Chami, R., Sutherland, M. D., Hall-Spencer, J. M., Lebleu, L., Benitez, M. B., and Levin, L. A.: The Role of Blue Carbon in Climate Change Mitigation and Carbon Stock Conservation, Frontiers in Climate, 3, https://doi.org/10.3389/fclim.2021.710546, 2021.

IPCC: Climate Change 2021: The Physical Science Basis. Contribution of Working Group I to the Sixth Assessment Report of the Intergovernmental Panel on Climate Change, vol. In Press, Cambridge University Press, Cambridge, United Kingdom and New York, NY, USA, https://doi.org/10.1017/9781009157896, 2021a.

IPCC: Summary for Policymakers, p. 3-32, Cambridge University Press, Cambridge, United Kingdom and New York, NY, USA, https://doi.org/10.1017/9781009157896.001, 2021b.

Jacobson, A. R., Mikaloff Fletcher, S. E., Gruber, N., Sarmiento, J. L., and Gloor, M.: A joint atmosphere-ocean inversion for surface fluxes of carbon dioxide: 2. Regional results, Global Biogeochemical Cycles, 21, https://doi.org/10.1029/2006GB002703, 2007.

Jiang, L., Yan, Y., Hararuk, O., Mikle, N., Xia, J., Shi, Z., Tjiputra, J., Wu, T., and Luo, Y.: Scale-Dependent Performance of CMIP5 Earth System Models in Simulating Terrestrial Vegetation Carbon, Journal of Climate, 28, 5217 – 5232, https://doi.org/10.1175/JCLI-D-14-00270.1, 2015.

Jiang, L., Liang, J., Lu, X., Hou, E., Hoffman, F. M., and Luo, Y.: Country-level land carbon sink and its causing components by the middle of the twenty-first century, Ecological Processes, 10, 61, https://doi.org/10.1186/s13717-021-00328-y, 2021.

Jiang, L.-Q., Carter, B. R., Feely, R. A., Lauvset, S. K., and Olsen, A.: Surface ocean pH and buffer capacity: past, present and future, Scientific Reports, 9, 18 624, https://doi.org/10.1038/s41598-019-55039-4, 2019.

Jones, C., Robertson, E., Arora, V., Friedlingstein, P., Shevliakova, E., Bopp, L., Brovkin, V., Hajima, T., Kato, E., Kawamiya, M., Liddicoat, S., Lindsay, K., Reick, C. H., Roelandt, C., Segschneider, J., and Tjiputra, J.: Twenty-First-Century Compatible CO_2 Emissions and Airborne Fraction Simulated by CMIP5 Earth System Models under Four Representative Concentration Pathways, Journal of Climate, 26, 4398 – 4413, https://doi.org/10.1175/JCLI-D-12-00554.1, 2013.

Jones, C. D., Hughes, J. K., Bellouin, N., Hardiman, S. C., Jones, G. S., Knight, J., Liddicoat, S., O'Connor, F. M., Andres, R. J., Bell, C., Boo, K.-O., Bozzo, A., Butchart, N., Cadule, P., Corbin, K. D., Doutriaux-Boucher, M., Friedlingstein, P., Gornall, J., Gray, L., Halloran, P. R., Hurtt, G., Ingram, W. J., Lamarque, J.-F., Law, R. M., Meinshausen, M., Osprey, S., Palin, E. J., Parsons Chini, L., Raddatz, T., Sanderson, M. G., Sellar, A. A., Schurer, A., Valdes, P., Wood, N., Woodward, S., Yoshioka, M., and Zerroukat, M.: The HadGEM2-ES implementation of CMIP5 centennial simulations, Geoscientific Model Development, 4, 543–570, https://doi.org/10.5194/gmd-4-543-2011, 2011.

Jones, C. D., Arora, V., Friedlingstein, P., Bopp, L., Brovkin, V., Dunne, J., Graven, H., Hoffman, F., Ilyina, T., John, J. G., Jung, M., Kawamiya, M., Koven, C., Pongratz, J., Raddatz, T., Randerson, J. T., and Zaehle, S.: C4MIP – The Coupled Climate–Carbon Cycle Model Intercomparison Project: experimental protocol for CMIP6, Geoscientific Model Development, 9, 2853–2880, https://doi.org/10.5194/gmd-9-2853-2016, 2016.

Katavouta, A. and Williams, R. G.: Ocean carbon cycle feedbacks in CMIP6 models: contributions from different basins, Biogeosciences, 18, 3189–3218, https://doi.org/10.5194/bg-18-3189-2021, 2021.

Koch, A., Hubau, W., and Lewis, S. L.: Earth System Models Are Not Capturing Present-Day Tropical Forest Carbon Dynamics, Earth's Future, 9, e2020EF001 874, https://doi.org/10.1029/2020EF001874, 2021.

Kroeker, K. J., Kordas, R. L., Crim, R., Hendriks, I. E., Ramajo, L., Singh, G. S., Duarte, C. M., and Gattuso, J.-P.: Impacts of ocean acidification on marine organisms: quantifying sensitivities and interaction with warming, Global Change Biology, 19, 1884–1896, https://doi.org/10.1111/gcb.12179, 2013.

Lawrence, D. M., Hurtt, G. C., Arneth, A., Brovkin, V., Calvin, K. V., Jones, A. D., Jones, C. D., Lawrence, P. J., de Noblet-Ducoudré, N., Pongratz, J., Seneviratne, S. I., and Shevliakova, E.: The Land Use Model Intercomparison Project (LUMIP) contribution to CMIP6: rationale and experimental design, Geoscientific Model Development, 9, 2973–2998, https://doi.org/10.5194/gmd-9-2973-2016, 2016.

Lawrence, M. G., Schäfer, S., Muri, H., Scott, V., Oschlies, A., Vaughan, N. E., Boucher, O., Schmidt, H., Haywood, J., and Scheffran, J.: Evaluating climate geoengineering proposals in the context of the Paris Agreement temperature goals, Nature Communications, 9, 3734, https://doi.org/10.1038/s41467-018-05938-3, 2018.

Le Quéré, C., Andrew, R. M., Friedlingstein, P., Sitch, S., Hauck, J., Pongratz, J., Pickers, P. A., Korsbakken, J. I., Peters, G. P., Canadell, J. G., Arneth, A., Arora, V. K., Barbero, L., Bastos, A., Bopp, L., Chevallier, F., Chini, L. P., Ciais, P., Doney, S. C., Gkritzalis, T., Goll,

D. S., Harris, I., Haverd, V., Hoffman, F. M., Hoppema, M., Houghton, R. A., Hurtt, G., Ilyina, T., Jain, A. K., Johannessen, T., Jones, C. D., Kato, E., Keeling, R. F., Goldewijk, K. K., Landschützer, P., Lefèvre, N., Lienert, S., Liu, Z., Lombardozzi, D., Metzl, N., Munro, D. R., Nabel, J. E. M. S., Nakaoka, S., Neill, C., Olsen, A., Ono, T., Patra, P., Peregon, A., Peters, W., Peylin, P., Pfeil, B., Pierrot, D., Poulter, B., Rehder, G., Resplandy, L., Robertson, E., Rocher, M., Rödenbeck, C., Schuster, U., Schwinger, J., Séférian, R., Skjelvan, I., Steinhoff, T., Sutton, A., Tans, P. P., Tian, H., Tilbrook, B., Tubiello, F. N., van der Laan-Luijkx, I. T., van der Werf, G. R., Viovy, N., Walker, A. P., Wiltshire, A. J., Wright, R., Zaehle, S., and Zheng, B.: Global Carbon Budget 2018, Earth System Science Data, 10, 2141–2194, https://doi.org/10.5194/essd-10-2141-2018, 2018.

Lee, J.-Y., Marotzke, J., Bala, G., Cao, L., Corti, S., Dunne, J., Engelbrecht, F., Fischer, E., Fyfe, J., Jones, C., Maycock, A., Mutemi, J., Ndiaye, O., Panickal, S., and Zhou, T.: Future Global Climate: Scenario-Based Projections and Near-Term Information, p. 553–672, Cambridge University Press, Cambridge, United Kingdom and New York, NY, USA, https://doi.org/10.1017/9781009157896.006, 2021.

Li, G., Cheng, L., Zhu, J., Trenberth, K. E., Mann, M. E., and Abraham, J. P.: Increasing ocean stratification over the past half-century, Nature Climate Change, 10, 1116–1123, https://doi.org/10.1038/s41558-020-00918-2, 2020.

Liddicoat, S. K., Wiltshire, A. J., Jones, C. D., Arora, V. K., Brovkin, V., Cadule, P., Hajima, T., Lawrence, D. M., Pongratz, J., Schwinger, J., Séférian, R., Tjiputra, J. F., and Ziehn, T.: Compatible Fossil Fuel CO_2 Emissions in the CMIP6 Earth System Models' Historical and Shared Socioeconomic Pathway Experiments of the Twenty-First Century, Journal of Climate, 34, 2853 – 2875, https://doi.org/10.1175/JCLI-D-19-0991.1, 2021.

Lovato, T., Peano, D., Butenschön, M., Materia, S., Iovino, D., Scoccimarro, E., Fogli, P. G., Cherchi, A., Bellucci, A., Gualdi, S., Masina, S., and Navarra, A.: CMIP6 Simulations With the CMCC Earth System Model (CMCC-ESM2), Journal of Advances in Modeling Earth Systems, 14, e2021MS002 814, https://doi.org/10.1029/2021MS002814, 2022.

Macreadie, P. I., Anton, A., Raven, J. A., Beaumont, N., Connolly, R. M., Friess, D. A., Kelleway, J. J., Kennedy, H., Kuwae, T., Lavery, P. S., Lovelock, C. E., Smale, D. A., Apostolaki, E. T., Atwood, T. B., Baldock, J., Bianchi, T. S., Chmura, G. L., Eyre, B. D., Fourqurean, J. W., Hall-Spencer, J. M., Huxham, M., Hendriks, I. E., Krause-Jensen, D., Laffoley, D., Luisetti, T., Marbà, N., Masque, P., McGlathery, K. J., Megonigal, J. P., Murdiyarso, D., Russell, B. D., Santos, R., Serrano, O., Silliman, B. R., Watanabe, K., and Duarte, C. M.: The future of Blue Carbon science, Nature Communications, 10, 3998, https://doi.org/10.1038/s41467-019-11693-w, 2019.

Mauritsen, T., Bader, J., Becker, T., Behrens, J., Bittner, M., Brokopf, R., Brovkin, V., Claussen, M., Crueger, T., Esch, M., Fast, I., Fiedler, S., Fläschner, D., Gayler, V., Giorgetta, M., Goll, D. S., Haak, H., Hagemann, S., Hedemann, C., Hohenegger, C., Ilyina, T., Jahns, T., Jimenéz-de-la Cuesta, D., Jungclaus, J., Kleinen, T., Kloster, S., Kracher, D., Kinne, S., Kleberg, D., Lasslop, G., Kornblueh, L., Marotzke, J., Matei, D., Meraner, K., Mikolajewicz, U., Modali, K., Möbis, B., Müller, W. A., Nabel, J. E. M. S., Nam, C. C. W., Notz, D., Nyawira, S.-S., Paulsen, H., Peters, K., Pincus, R., Pohlmann, H., Pongratz, J., Popp, M., Raddatz, T. J., Rast, S., Redler, R., Reick, C. H., Rohrschneider, T., Schemann, V., Schmidt, H., Schnur, R., Schulzweida, U., Six, K. D., Stein, L., Stemmler, I., Stevens, B., von Storch, J.-S., Tian, F., Voigt, A., Vrese, P., Wieners, K.-H., Wilkenskjeld, S., Winkler, A., and Roeckner, E.: Developments in the MPI-M Earth System Model version 1.2 (MPI-ESM1.2) and Its Response to Increasing CO_2, Journal of Advances in Modeling Earth Systems, 11, 998–1038, https://doi.org/10.1029/2018MS001400, 2019.

Meehl, G. A., Senior, C. A., Eyring, V., Flato, G., Lamarque, J.-F., Stouffer, R. J., Taylor, K. E., and Schlund, M.: Context for interpreting equilibrium climate sensitivity and transient climate response from the CMIP6 Earth system models, Science Advances, 6, eaba1981, https://doi.org/10.1126/sciadv.aba1981, 2020.

Meinshausen, M., Vogel, E., Nauels, A., Lorbacher, K., Meinshausen, N., Etheridge, D. M., Fraser, P. J., Montzka, S. A., Rayner, P. J., Trudinger, C. M., Krummel, P. B., Beyerle, U., Canadell, J. G., Daniel, J. S., Enting, I. G., Law, R. M., Lunder, C. R., O'Doherty, S.,

Prinn, R. G., Reimann, S., Rubino, M., Velders, G. J. M., Vollmer, M. K., Wang, R. H. J., and Weiss, R.: Historical greenhouse gas concentrations for climate modelling (CMIP6), Geoscientific Model Development, 10, 2057–2116, https://doi.org/10.5194/gmd-10-2057-2017, 2017.

Meinshausen, M., Nicholls, Z. R. J., Lewis, J., Gidden, M. J., Vogel, E., Freund, M., Beyerle, U., Gessner, C., Nauels, A., Bauer, N., Canadell, J. G., Daniel, J. S., John, A., Krummel, P. B., Luderer, G., Meinshausen, N., Montzka, S. A., Rayner, P. J., Reimann, S., Smith, S. J., van den Berg, M., Velders, G. J. M., Vollmer, M. K., and Wang, R. H. J.: The shared socio-economic pathway (SSP) greenhouse gas concentrations and their extensions to 2500, Geoscientific Model Development, 13, 3571–3605, https://doi.org/10.5194/gmd-13-3571-2020, 2020.

Muilwijk, M., Nummelin, A., Heuzé, C., Polyakov, I. V., Zanowski, H., and Smedsrud, L. H.: Divergence in Climate Model Projections of Future Arctic Atlantification, Journal of Climate, 36, 1727 – 1748, https://doi.org/10.1175/JCLI-D-22-0349.1, 2023.

Myers, N.: Carbon Dioxide Review, Environmental Conservation, 10, 370–371, https://doi.org/10.1017/S0376892900013345, 1983.

Nyberg, M. and Hovenden, M. J.: Warming increases soil respiration in a carbon-rich soil without changing microbial respiratory potential, Biogeosciences, 17, 4405–4420, https://doi.org/10.5194/bg-17-4405-2020, 2020.

O'Neill, B. C., Tebaldi, C., van Vuuren, D. P., Eyring, V., Friedlingstein, P., Hurtt, G., Knutti, R., Kriegler, E., Lamarque, J.-F., Lowe, J., Meehl, G. A., Moss, R., Riahi, K., and Sanderson, B. M.: The Scenario Model Intercomparison Project (ScenarioMIP) for CMIP6, Geoscientific Model Development, 9, 3461–3482, https://doi.org/10.5194/gmd-9-3461-2016, 2016.

Pongratz, J., Reick, C. H., Houghton, R. A., and House, J. I.: Terminology as a key uncertainty in net land use and land cover change carbon flux estimates, Earth System Dynamics, 5, 177–195, https://doi.org/10.5194/esd-5-177-2014, 2014.

Raupach, M. R., Gloor, M., Sarmiento, J. L., Canadell, J. G., Frölicher, T. L., Gasser, T., Houghton, R. A., Le Quéré, C., and Trudinger, C. M.: The declining uptake rate of atmospheric CO_2 by land and ocean sinks, Biogeosciences, 11, 3453–3475, https://doi.org/10.5194/bg-11-3453-2014, 2014.

Resplandy, L., Keeling, R., Rödenbeck, C., Stephens, B. B., Khatiwala, S., Rodgers, K., Long, M. C., Bopp, L., and Tans, P. P.: Revision of global carbon fluxes based on a reassessment of oceanic and riverine carbon transport, Nature Geoscience, 11, 504—509, https://doi.org/10.1038/s41561-018-0151-3, 2018.

Riahi, K., van Vuuren, D. P., Kriegler, E., Edmonds, J., O'Neill, B. C., Fujimori, S., Bauer, N., Calvin, K., Dellink, R., Fricko, O., Lutz, W., Popp, A., Cuaresma, J. C., KC, S., Leimbach, M., Jiang, L., Kram, T., Rao, S., Emmerling, J., Ebi, K., Hasegawa, T., Havlik, P., Humpenöder, F., Da Silva, L. A., Smith, S., Stehfest, E., Bosetti, V., Eom, J., Gernaat, D., Masui, T., Rogelj, J., Strefler, J., Drouet, L., Krey, V., Luderer, G., Harmsen, M., Takahashi, K., Baumstark, L., Doelman, J. C., Kainuma, M., Klimont, Z., Marangoni, G., Lotze-Campen, H., Obersteiner, M., Tabeau, A., and Tavoni, M.: The Shared Socioeconomic Pathways and their energy, land use, and greenhouse gas emissions implications: An overview, Global Environmental Change, 42, 153–168, https://doi.org/10.1016/j.gloenvcha.2016.05.009, 2017.

Righi, M., Andela, B., Eyring, V., Lauer, A., Predoi, V., Schlund, M., Vegas-Regidor, J., Bock, L., Brötz, B., de Mora, L., Diblen, F., Dreyer, L., Drost, N., Earnshaw, P., Hassler, B., Koldunov, N., Little, B., Loosveldt Tomas, S., and Zimmermann, K.: Earth System Model Evaluation Tool (ESMValTool) v2.0 – technical overview, Geoscientific Model Development, 13, 1179–1199, https://doi.org/10.5194/gmd-13-1179-2020, 2020.

Roser, M. and Ritchie, H.: Oil Spills, Our World in Data, https://ourworldindata.org/oil-spills, Accessed: 2023-09-11, 2023.

Sallée, J.-B., Pellichero, V., Akhoudas, C., Pauthenet, E., Vignes, L., Schmidtko, S., Garabato, A. N., Sutherland, P., and Kuusela, M.: Summertime increases in upper-ocean stratification and mixed-layer depth, Nature, 591, 592–598, https://doi.org/10.1038/s41586-021-03303-x, 2021.

Scafetta, N.: Advanced Testing of Low, Medium, and High ECS CMIP6 GCM Simulations Versus ERA5-T2m, Geophysical Research Letters, 49, e2022GL097 716, https://doi.org/10.1029/2022GL097716, 2022.

Schlunegger, S., Rodgers, K. B., Sarmiento, J. L., Frölicher, T. L., Dunne, J. P., Ishii, M., and Slater, R.: Emergence of anthropogenic signals in the ocean carbon cycle, Nature Climate Change, 9, 719–725, https://doi.org/10.1038/s41558-019-0553-2, 2019.

Sellar, A. A., Walton, J., Jones, C. G., Wood, R., Abraham, N. L., Andrejczuk, M., Andrews, M. B., Andrews, T., Archibald, A. T., de Mora, L., Dyson, H., Elkington, M., Ellis, R., Florek, P., Good, P., Gohar, L., Haddad, S., Hardiman, S. C., Hogan, E., Iwi, A., Jones, C. D., Johnson, B., Kelley, D. I., Kettleborough, J., Knight, J. R., Köhler, M. O., Kuhlbrodt, T., Liddicoat, S., Linova-Pavlova, I., Mizielinski, M. S., Morgenstern, O., Mulcahy, J., Neininger, E., O'Connor, F. M., Petrie, R., Ridley, J., Rioual, J.-C., Roberts, M., Robertson, E., Rumbold, S., Seddon, J., Shepherd, H., Shim, S., Stephens, A., Teixiera, J. C., Tang, Y., Williams, J., Wiltshire, A., and Griffiths, P. T.: Implementation of U.K. Earth System Models for CMIP6, Journal of Advances in Modeling Earth Systems, 12, e2019MS001 946, https://doi.org/10.1029/2019MS001946, 2020.

Sherwood, S. C., Webb, M. J., Annan, J. D., Armour, K. C., Forster, P. M., Hargreaves, J. C., Hegerl, G., Klein, S. A., Marvel, K. D., Rohling, E. J., Watanabe, M., Andrews, T., Braconnot, P., Bretherton, C. S., Foster, G. L., Hausfather, Z., von der Heydt, A. S., Knutti, R., Mauritsen, T., Norris, J. R., Proistosescu, C., Rugenstein, M., Schmidt, G. A., Tokarska, K. B., and Zelinka, M. D.: An Assessment of Earth's Climate Sensitivity Using Multiple Lines of Evidence, Reviews of Geophysics, 58, e2019RG000 678, https://doi.org/10.1029/2019RG000678, 2020.

Smith, C. J., Kramer, R. J., Myhre, G., Alterskjær, K., Collins, W., Sima, A., Boucher, O., Dufresne, J.-L., Nabat, P., Michou, M., Yukimoto, S., Cole, J., Paynter, D., Shiogama, H., O'Connor, F. M., Robertson, E., Wiltshire, A., Andrews, T., Hannay, C., Miller, R., Nazarenko, L., Kirkevåg, A., Olivié, D., Fiedler, S., Lewinschal, A., Mackallah, C., Dix, M., Pincus, R., and Forster, P. M.: Effective radiative forcing and adjustments in CMIP6 models, Atmospheric Chemistry and Physics, 20, 9591–9618, https://doi.org/10.5194/acp-20-9591-2020, 2020.

Sullivan, A., Baker, E., and Kurvits, T.: Spreading Like Wildfire: The Rising Threat of Extraordinary Landscape Fires, Tech. rep., UN Environment Program, https://policycommons.net/artifacts/2259313/wildfire_rra, accessed 2023-09-11, 2022.

Swaminathan, R., Parker, R. J., Jones, C. G., Allan, R. P., Quaife, T., Kelley, D. I., de Mora, L., and Walton, J.: The Physical Climate at Global Warming Thresholds as Seen in the U.K. Earth System Model, Journal of Climate, 35, 29 – 48, https://doi.org/10.1175/JCLI-D-21-0234.1, 2022.

Swart, N. C., Cole, J. N. S., Kharin, V. V., Lazare, M., Scinocca, J. F., Gillett, N. P., Anstey, J., Arora, V., Christian, J. R., Hanna, S., Jiao, Y., Lee, W. G., Majaess, F., Saenko, O. A., Seiler, C., Seinen, C., Shao, A., Sigmond, M., Solheim, L., von Salzen, K., Yang, D., and Winter, B.: The Canadian Earth System Model version 5 (CanESM5.0.3), Geoscientific Model Development, 12, 4823–4873, https://doi.org/10.5194/gmd-12-4823-2019, 2019.

Tebaldi, C., Debeire, K., Eyring, V., Fischer, E., Fyfe, J., Friedlingstein, P., Knutti, R., Lowe, J., O'Neill, B., Sanderson, B., van Vuuren, D., Riahi, K., Meinshausen, M., Nicholls, Z., Tokarska, K. B., Hurtt, G., Kriegler, E., Lamarque, J.-F., Meehl, G., Moss, R., Bauer, S. E., Boucher, O., Brovkin, V., Byun, Y.-H., Dix, M., Gualdi, S., Guo, H., John, J. G., Kharin, S., Kim, Y., Koshiro, T., Ma, L., Olivié, D., Panickal, S., Qiao, F., Rong, X., Rosenbloom, N., Schupfner, M., Séférian, R., Sellar, A., Semmler, T., Shi, X., Song, Z., Steger, C., Stouffer, R., Swart, N., Tachiiri, K., Tang, Q., Tatebe, H., Voldoire, A., Volodin, E., Wyser, K., Xin, X., Yang, S., Yu, Y., and Ziehn, T.: Climate model projections from the Scenario Model Intercomparison Project (ScenarioMIP) of CMIP6, Earth System Dynamics, 12, 253–293, https://doi.org/10.5194/esd-12-253-2021, 2021.

Thibodeau, B., Not, C., Zhu, J., Schmittner, A., Noone, D., Tabor, C., Zhang, J., and Liu, Z.: Last Century Warming Over the Canadian Atlantic Shelves Linked to Weak Atlantic Meridional Overturning Circulation, Geophysical Research Letters, 45, 12,376–12,385, https://doi.org/10.1029/2018GL080083, 2018.

Twomey, S.: The Influence of Pollution on the Shortwave Albedo of Clouds, Journal of Atmospheric Sciences, 34, 1149 – 1152, https://doi.org/10.1175/1520-0469(1977)034<1149:TIOPOT>2.0.CO;2, 1977.

Ukkola, A. M., Prentice, I., Keenan, T. F., van Dijk, A. I., Viney, N. R., Myneni, R., and Bi, J.: Reduced streamflow in water-stressed climates consistent with CO_2 effects on vegetation, Nature Climate Change, 6, 75–78, https://doi.org/10.1038/nclimate2831, 2016.

United Nations: Transforming our world : the 2030 Agenda for Sustainable Development, p. 35 p., http://digitallibrary.un.org/record/3923923, issued in GAOR, 70th sess., Suppl. no. 49., 2015.

United Nations Environment Programme: Emissions Gap Report 2019, https://wedocs.unep.org/20.500.11822/30797, accessed 2023-09-11, 2019.

United Nations Treaty Collection: Paris Agreement, https://treaties.un.org/pages/ViewDetails.aspx?src=TREATY&mtdsg_no=XXVII-7-d&chapter=27&clang=_en, 2015.

van der Molen, M., Dolman, A., Ciais, P., Eglin, T., Gobron, N., Law, B., Meir, P., Peters, W., Phillips, O., Reichstein, M., Chen, T., Dekker, S., Doubková, M., Friedl, M., Jung, M., van den Hurk, B., de Jeu, R., Kruijt, B., Ohta, T., Rebel, K., Plummer, S., Seneviratne, S., Sitch, S., Teuling, A., van der Werf, G., and Wang, G.: Drought and ecosystem carbon cycling, Agricultural and Forest Meteorology, 151, 765–773, https://doi.org/10.1016/j.agrformet.2011.01.018, 2011.

Wang, S., Zhang, Y., Ju, W., Chen, J. M., Ciais, P., Cescatti, A., Sardans, J., Janssens, I. A., Wu, M., Berry, J. A., Campbell, E., Fernández-Martínez, M., Alkama, R., Sitch, S., Friedlingstein, P., Smith, W. K., Yuan, W., He, W., Lombardozzi, D., Kautz, M., Zhu, D., Lienert, S., Kato, E., Poulter, B., Sanders, T. G. M., Krüger, I., Wang, R., Zeng, N., Tian, H., Vuichard, N., Jain, A. K., Wiltshire, A., Haverd, V., Goll, D. S., and Peñuelas, J.: Recent global decline of CO_2 fertilization effects on vegetation photosynthesis, Science, 370, 1295–1300, https://doi.org/10.1126/science.abb7772, 2020.

Watson, A. J., Schuster, U., Shutler, J. D., Holding, T., Ashton, I. G. C., Landschützer, P., Woolf, D. K., and Goddijn-Murphy, L.: Revised estimates of ocean-atmosphere CO_2 flux are consistent with ocean carbon inventory, Nature Communications, 11, 4422, https://doi.org/10.1038/s41467-020-18203-3, 2020.

Weijer, W., Cheng, W., Garuba, O. A., Hu, A., and Nadiga, B. T.: CMIP6 Models Predict Significant 21st Century Decline of the Atlantic Meridional Overturning Circulation, Geophysical Research Letters, 47, e2019GL086 075, https://doi.org/10.1029/2019GL086075, 2020.

World Bank: Turn Down the Heat: Why a 4°C Warmer World Must Be Avoided, http://documents.worldbank.org/curated/en/865571468149107611/Turn-down-the-heat-why-a-4-C-warmer-world-must-be-avoided, accessed 2023-09-11, 2012.

Yool, A., Palmiéri, J., Jones, C. G., Sellar, A. A., de Mora, L., Kuhlbrodt, T., Popova, E. E., Mulcahy, J. P., Wiltshire, A., Rumbold, S. T., Stringer, M., Hill, R. S. R., Tang, Y., Walton, J., Blaker, A., Nurser, A. J. G., Coward, A. C., Hirschi, J., Woodward, S., Kelley, D. I., Ellis, R., and Rumbold-Jones, S.: Spin-up of UK Earth System Model 1 (UKESM1) for CMIP6, Journal of Advances in Modeling Earth Systems, 12, e2019MS001 933, https://doi.org/10.1029/2019MS001933, 2020.

Zeebe, R. E.: History of Seawater Carbonate Chemistry, Atmospheric CO_2, and Ocean Acidification, Annual Review of Earth and Planetary Sciences, 40, 141–165, https://doi.org/10.1146/annurev-earth-042711-105521, 2012.

Zelinka, M. D., Myers, T. A., McCoy, D. T., Po-Chedley, S., Caldwell, P. M., Ceppi, P., Klein, S. A., and Taylor, K. E.: Causes of Higher Climate Sensitivity in CMIP6 Models, Geophysical Research Letters, 47, e2019GL085 782, https://doi.org/10.1029/2019GL085782, 2020.

Ziehn, T., Chamberlain, M. A., Law, R. M., Lenton, A., Bodman, R. W., Dix, M., Stevens, L., Wang, Y.-P., and Srbinovsky, J.: The Australian Earth System Model: ACCESS-ESM1.5, Journal of Southern Hemisphere Earth Systems Science, 70, 193–214, https://doi.org/10.1071/ES19035, 2020.